

# DLPNO-MP2 with Periodic Boundary Conditions

Arman Nejad, Andrew Zhu, Kesha Sorathia, and David P. Tew\*

*University of Oxford, South Parks Road, Oxford, OX1 3QZ, UK*

(Dated: July 15, 2025)

We present domain-based local pair natural orbital Møller–Plesset second order perturbation theory (DLPNO-MP2) with Born–von Kármán boundary (BvK) conditions. The approach is based on well-localised Wannier functions in a LCAO formalism and extends the molecular DLPNO-MP2 implementation Tubromole program package to periodic systems. The PNOs are formed through a PAO-OSV-PNO cascade, using BvK projected atomic orbitals and orbital specific virtuals as intermediaries in an analogous manner to the molecular scheme. Our chargeless and surface-dipole corrected local density fitting approach is shown to be numerically stable and to ensure convergent lattice summations over the periodic images for the two- and three-index Coulomb integrals. Through careful benchmarking, we show that the DLPNO approximations in the BvK-DLPNO-MP2 methods are entirely consistent with those of molecular DLPNO-MP2 calculations, and with an alternative periodic approach Megacell-DLPNO-MP2, reported in Paper II of this series. Smooth convergence to the canonical correlation energy with tightening PNO threshold is observed. Reference MP2 correlation energies are provided for a set of 2D and 3D periodic systems using a triple-zeta basis and supercell sizes up to  $11 \times 11$  and  $7 \times 7 \times 7$ .

## I. INTRODUCTION

Computational studies of the electronic structure of materials are currently predominantly performed using density functional theory (DFT),<sup>1,2</sup> due to its excellent cost-to-accuracy ratio. The need to surmount the uncertainties inherent in DFT predictions has motivated several research groups to explore the systematically improvable set of post-Hartree–Fock (HF) correlated wavefunction-based methods. In particular, periodic implementations of Møller–Plesset perturbation theory<sup>3–7</sup> and coupled cluster methods<sup>8–10</sup> are now available and have been applied to study the structure and stability of materials and surface processes.<sup>4,6,8,10–27</sup>

The primary challenge in using accurate wavefunction approaches for materials is the computational expense. Canonical second-order Møller–Plesset perturbation theory (MP2) scales as  $\mathcal{O}(N^5)$  with system size, whilst canonical coupled cluster with singles, doubles and perturbative triples (CCSD(T)) scales as  $\mathcal{O}(N^7)$ . The large simulations required to converge the correlation treatment to the thermodynamic limit quickly become prohibitively expensive. Local correlation approximations provide a solution to this problem for insulating materials. For example, the pioneering work by Pisani and Schütz and coworkers in the Cryscor program<sup>4,11,12,28–30</sup> leverages projected atomic orbitals<sup>31</sup> (PAOs) and orbital specific virutals<sup>32</sup> (OSVs) to obtain a low-scaling MP2 implementation for non-conducting systems using atom-centred Gaussian basis functions. More recently, Ye and Berkelbach<sup>18</sup> have adapted Kállay’s local natural orbital (LNOs) approach<sup>33–36</sup> to periodic systems, at the CCSD and CCSD(T) levels of theory, also in a linear combination of atomic orbitals (LCAO) framework. These methods have been applied successfully to obtain properties

such as lattice constants, cohesive energies<sup>12,18,37</sup> and adsorption energies<sup>10,27,38,39</sup> for surface interactions.

This paper concerns the extension of domain-based pair natural orbital local correlation (DLPNO) theory<sup>40,41</sup> to periodic systems. DLPNO theory achieves near-linear scaling of computational effort with system size, with only modest loss in accuracy, by replacing Hamiltonian integrals and excitation amplitudes with low-rank approximations that exploit the inherent locality of electron correlation in insulators. DLPNO theory within an LCAO framework has been highly successful in the molecular setting where it has been extended to perturbative<sup>42–46</sup> and coupled cluster formalisms<sup>47–55</sup>, to explicitly correlated theory<sup>45,56–59</sup>, to multireference methods<sup>60–62</sup> and to excited states,<sup>63–65</sup> greatly extending the range of applicability of these approaches for computing energies and properties. The pair-specific nature of PNOs affords a much greater degree of compression of the correlation space than PAOs or OSVs, where domains for distant pairs are the same size as for close pairs.

We are concurrently pursuing two complementary approaches to simulating periodic systems using DLPNO correlation theory. One where Born–von Kármán (BvK) boundary conditions<sup>66,67</sup> are applied to the correlation treatment, leading to electron repulsion integrals involving lattice summations over infinite periodic images, and one that embeds a supercell correlation treatment in a much larger megacell, where integrals do not involve lattice summations and periodicity is imposed through translational invariance. The Megacell approach is presented in Paper II of this series;<sup>68</sup> this paper details the BvK scheme. We provide the full working equations for DLPNO-MP2 theory, starting from periodic PAOs through OSVs, to PNOs. We detail the necessary modifications to the local density fitting method for obtaining electron repulsion integrals (ERIs) under BvK boundary conditions,<sup>69–71</sup> where it is essential to project out the charged contributions and to remove the spurious surface

\* Email: david.tew@chem.ox.ac.uk

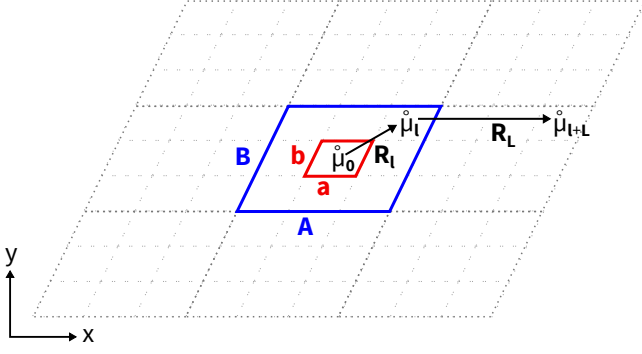


FIG. 1: Definition of a 2D BvK supercell (blue box) which is composed of  $\mathcal{N} = \mathcal{N}_a \cdot \mathcal{N}_b = 9$  unit cells (red box).

TABLE I: Summary on index convention.

$i, j, k, \dots$	Active occupied orbital
$a, b, c, \dots$	Active virtual orbital
$\tilde{\mu}, \tilde{\nu}, \dots$	PAO
$\tilde{a}, \tilde{b}, \dots$	PNO or OSV
$\bar{a}, \bar{b}, \dots$	pre-PNO
$\mu, \nu, \kappa, \dots$	AO
$P, Q, \dots$	Auxiliary DF functions
$\mathbf{k}$	Crystal momentum
$\mathbf{l}, \mathbf{m}, \mathbf{n}$	Lattice vector index of unit cell in BvK cell
$\mathbf{L}, \mathbf{M}, \mathbf{N}$	Lattice vector index of BvK cell in crystal
$\mathcal{N} = \mathcal{N}_a \mathcal{N}_b \mathcal{N}_c$	Number of unit cells in BvK cell
$\mathbf{a}, \mathbf{b}, \mathbf{c}$	Lattice vectors of unit cell
$\mathbf{A}, \mathbf{B}, \mathbf{C}$	Lattice vectors of BvK cell
$\mathbf{R}_l$	$l_a \mathbf{a} + l_b \mathbf{b} + l_c \mathbf{c}$
$\mathbf{R}_L$	$L_a \mathbf{A} + L_b \mathbf{B} + L_c \mathbf{C}$
$\mu_{\mathbf{k}}$	Bloch AO
$\mu_l$	BvK AO
$\dot{\mu}_{l+\mathbf{L}}$	Individual AO

energy that arises from dipole-dipole terms.<sup>11,28,69,72–76</sup> We present benchmark calculations validating the implementation and demonstrate that the PNO approximations are equally applicable in the molecular and periodic settings. Our implementation leverages the existing molecular DLPNO-MP2 code<sup>43</sup> in the Turbomole program package and is made possible due to the periodic Hartree–Fock implementation in the `riper` module.<sup>77,78</sup> We report triple-zeta quality MP2 energies for a set of 2D and 3D periodic systems, computed using supercell sizes up to  $11 \times 11$  and  $7 \times 7 \times 7$  and involving nearly 5000 functions in the correlation treatment.

## II. LOCAL MP2 WITH PERIODIC BOUNDARY CONDITIONS

We are working in the LCAO formulation of Hartree–Fock theory with Born–von Kármán boundary condi-

tions. The basis functions are BvK AOs

$$\mu_l(\mathbf{r}) = \sum_{\mathbf{L}} \dot{\mu}(\mathbf{r} - \mathbf{R}_l - \mathbf{R}_L) = \sum_{\mathbf{L}} \dot{\mu}_{l+\mathbf{L}}(\mathbf{r}) \quad (1)$$

Here  $\mu$  labels the AO within a unit cell and  $\mathbf{l}$  is a vector index labelling the unit cell in the BvK supercell. The BvK AO has the periodicity of the BvK supercell since it is the infinite sum over all periodic images of the AO  $\dot{\mu}$  at  $\mathbf{R}_L$  where  $\mathbf{L}$  is the vector index labelling the supercell within the infinite crystal. Table I and Figure 1 summarise the index conventions used in this paper. Hartree–Fock calculations are performed in the basis of Bloch AOs, which are eigenfunctions of the momentum operator with eigenvalue  $\mathbf{k}$

$$\mu_{\mathbf{k}}(\mathbf{r}) = \frac{1}{\sqrt{\mathcal{N}}} \sum_{\mathbf{l}} e^{i\mathbf{k} \cdot \mathbf{R}_l} \mu_l(\mathbf{r}) \quad (2)$$

Here  $\mathbf{R}_l$  is the lattice position of unit cell  $\mathbf{l}$  in the BvK supercell and  $\mathcal{N} = \mathcal{N}_a \mathcal{N}_b \mathcal{N}_c$  is the number of unit cells in the BvK supercell. The BvK boundary condition imposes discretisation on the momenta  $\mathbf{k}$ . In this work we adopt the Monkhorst-Pack  $k$ -point grid.<sup>79</sup> The conversion between BvK AOs and Bloch AOs is in this case a generalised discrete Fourier transform (FT) and our choice of normalisation is such that the FT matrix is unitary

$$V_l^{\mathbf{k}} = \frac{1}{\sqrt{\mathcal{N}}} e^{i\mathbf{k} \cdot \mathbf{R}_l} \quad (3)$$

The overlap and Fock matrices are block diagonal in the Bloch AO basis and the Hartree–Fock orbitals and eigenvalues satisfy

$$\mathbf{F}_{\mathbf{k}}^{\mathbf{k}} \mathbf{C}_{\mathbf{k}}^{\mathbf{k}} = \mathbf{S}_{\mathbf{k}}^{\mathbf{k}} \mathbf{C}_{\mathbf{k}}^{\mathbf{k}} \epsilon_{\mathbf{k}} \quad (4)$$

where

$$\langle \mu_{\mathbf{k}} | \nu_{\mathbf{k}'} \rangle_{\text{BvK}} = \delta_{\mathbf{k}\mathbf{k}'} S_{\mu_{\mathbf{k}}}^{\nu_{\mathbf{k}'}} \quad (5)$$

$$\langle \mu_{\mathbf{k}} | \hat{F} | \nu_{\mathbf{k}'} \rangle_{\text{BvK}} = \delta_{\mathbf{k}\mathbf{k}'} F_{\mu_{\mathbf{k}}}^{\nu_{\mathbf{k}'}} \quad (6)$$

The BvK subscript indicates integrals over the BvK supercell. Solution of the HF equations yields the canonical molecular orbitals (MOs)  $|p_{\mathbf{k}}\rangle$  and orbital eigenvalues  $\epsilon_{p_{\mathbf{k}}}$ . The spin-free MP2 amplitude and energy equations are

$$0 = g_{a_{\mathbf{k}_3} b_{\mathbf{k}_4}}^{i_{\mathbf{k}_1} j_{\mathbf{k}_2}} + (\epsilon_{a_{\mathbf{k}_3}} + \epsilon_{b_{\mathbf{k}_4}} - \epsilon_{i_{\mathbf{k}_1}} - \epsilon_{j_{\mathbf{k}_2}}) t_{a_{\mathbf{k}_3} b_{\mathbf{k}_4}}^{i_{\mathbf{k}_1} j_{\mathbf{k}_2}} \quad (7)$$

$$E_{\text{corr}} = \frac{1}{\mathcal{N}} \sum_{i_{\mathbf{k}_1} j_{\mathbf{k}_2}} \sum_{a_{\mathbf{k}_3} b_{\mathbf{k}_4}} (2g_{i_{\mathbf{k}_1} j_{\mathbf{k}_2}}^{a_{\mathbf{k}_3} b_{\mathbf{k}_4}} - g_{i_{\mathbf{k}_1} j_{\mathbf{k}_2}}^{b_{\mathbf{k}_4} a_{\mathbf{k}_3}}) t_{a_{\mathbf{k}_3} b_{\mathbf{k}_4}}^{i_{\mathbf{k}_1} j_{\mathbf{k}_2}} \quad (8)$$

where  $E_{\text{corr}}$  is the correlation energy per unit cell and  $g_{i_{\mathbf{k}_1} j_{\mathbf{k}_2}}^{a_{\mathbf{k}_3} b_{\mathbf{k}_4}} = \langle i_{\mathbf{k}_1} j_{\mathbf{k}_2} | a_{\mathbf{k}_3} b_{\mathbf{k}_4} \rangle_{\text{BvK}}$  are the BvK electron repulsion integrals.

The coefficients of the canonical MOs  $|p_{\mathbf{k}}\rangle$  in the BvK AO basis are the inverse FT of the Bloch AO coefficients

in the Fock equation

$$C_{\mu_{\mathbf{m}}}^{p_{\mathbf{k}}} = \sum_{\mathbf{k}'} \delta_{\mathbf{k}\mathbf{k}'} C_{\mu_{\mathbf{k}'}}^{p_{\mathbf{k}}} V_{\mathbf{m}}^{\mathbf{k}'} \quad (9)$$

These Bloch MOs are delocalised throughout the BvK supercell and are not suitable for local correlation approximations. To obtain functions that are localised on a unit cell a further inverse FT is performed on the Bloch MOs to obtain Wannier functions  $|p_1\rangle$  with coefficients

$$C_{\mu_{\mathbf{m}}}^{p_1} = \sum_{\mathbf{k}} C_{\mu_{\mathbf{m}}}^{p_{\mathbf{k}}} V_{\mathbf{l}}^{\mathbf{k}} \quad (10)$$

Wannier functions can be further localised by rotating the Bloch MOs  $|p_{\mathbf{k}}\rangle$  for each  $k$ -point among themselves before wannierisation and finding the unitary matrix that maximises a chosen locality metric. We have recently introduced a procedure for obtaining well localised Wannier functions by optimising a fourth-order Pipek–Mezey metric using atomic charges from Bloch intrinsic atomic orbitals,<sup>80</sup> which we summarise in Section III. In the Wannier basis, the MP2 energy and amplitude equations become

$$0 = g_{a_{13}b_{14}}^{i_{11}j_{12}} + \sum_{c_{15}} (f_{a_{13}c_{15}b_{14}}^{i_{11}j_{12}} + f_{b_{12}c_{15}a_{13}}^{i_{11}j_{12}}) - \sum_{k_{15}} (t_{a_{13}b_{14}k_{15}}^{i_{11}j_{12}} + t_{a_{13}b_{14}k_{15}}^{i_{11}k_{15}} f_{k_{15}}^{j_{12}}) \quad (11)$$

$$E_{\text{corr}} = \frac{1}{\mathcal{N}} \sum_{i_{11}j_{12}} \sum_{a_{13}b_{14}} (2g_{a_{13}b_{14}}^{i_{11}j_{12}} - g_{b_{14}a_{13}}^{i_{11}j_{12}}) t_{a_{13}b_{14}}^{i_{11}j_{12}} \quad (12)$$

where the electron repulsion integrals in the BvK AO basis are evaluated as

$$\langle \mu_{l_1} \nu_{l_2} | \kappa_{l_3} \lambda_{l_4} \rangle_{\text{BvK}} = \sum_{\mathbf{L}_2 \mathbf{L}_3 \mathbf{L}_4}^{\infty} \langle \mu_{l_1} \nu_{\mathbf{L}_2+\mathbf{l}_2} | \kappa_{\mathbf{L}_3+\mathbf{l}_3} \lambda_{\mathbf{L}_4+\mathbf{l}_4} \rangle \quad (13)$$

Wannier functions are translationally invariant  $C_{\mu_{\mathbf{m}+\mathbf{l}}}^{p_{\mathbf{o}}} = C_{\mu_{\mathbf{m}}}^{p_1}$ , where it is understood that  $\mathbf{m}+\mathbf{l}$  implies modulo arithmetic around the BvK supercell. All integrals and amplitudes inherit this same translational symmetry. It is therefore only necessary to compute the residual for  $t_{a_{\mathbf{m}}b_{\mathbf{n}}}^{i_{\mathbf{o}}j_{\mathbf{l}}}$  where  $\mathbf{o}$  is the reference unit cell. The correlation energy per unit cell is

$$E_{\text{corr}} = \frac{2}{1 + \delta_{i_{\mathbf{o}}j_{\mathbf{l}}}} \sum_{i_{\mathbf{o}} \leq j_{\mathbf{l}}} \sum_{a_{\mathbf{m}}b_{\mathbf{n}}} (2g_{a_{\mathbf{m}}b_{\mathbf{n}}}^{i_{\mathbf{o}}j_{\mathbf{l}}} - g_{b_{\mathbf{m}}a_{\mathbf{n}}}^{i_{\mathbf{o}}j_{\mathbf{l}}}) t_{a_{\mathbf{m}}b_{\mathbf{n}}}^{i_{\mathbf{o}}j_{\mathbf{l}}} \quad (14)$$

where the restricted summation counts each pair interaction once and only includes pairs where at least one orbital is in the reference unit cell. The Fock matrix elements in the Wannier basis can be obtained from the band energies

$$f_{p_1}^{q_{\mathbf{m}}} = \sum_{\mathbf{k}} V_{\mathbf{l}}^{\mathbf{k}} f_{p_{\mathbf{k}}}^{q_{\mathbf{k}}} V_{\mathbf{m}}^{\mathbf{k}} \quad (15)$$

$$\mathbf{f}_{\mathbf{k}}^{\mathbf{k}} = \mathbf{U}_{\mathbf{k}}^{\dagger} \mathbf{F}_{\mathbf{k}}^{\mathbf{k}} \mathbf{U}_{\mathbf{k}}^{\mathbf{k}} \quad (16)$$

where  $\mathbf{U}_{\mathbf{k}}^{\mathbf{k}}$  are the unitary matrices that mix the bands at each  $k$ -point to maximise the chosen locality metric.

The Wannier functions are localised at a unit cell and local approximations can be applied. Specifically, PAO, OSV and PNO approaches can be applied to generate an  $\mathcal{O}(1)$  set of localised virtual orbitals  $\{\tilde{a}_{i_{\mathbf{o}}j_{\mathbf{l}}}\}$  adapted to describe the correlation of pair  $i_{\mathbf{o}}j_{\mathbf{l}}$ . In addition, distant electrons in orbitals  $j_{\mathbf{l}}$  have negligible correlation with electrons in orbital  $i_{\mathbf{o}}$  of the reference unit cell and the number of significant pairs  $i_{\mathbf{o}}j_{\mathbf{l}}$  with pair energy greater than  $\epsilon$  tends to a constant as the size of the BvK supercell is increased.

### III. WELL-LOCALISED WANNIER FUNCTIONS

#### A. Diabatic Wannier Functions

Bloch functions are only determined up to an arbitrary phase, or gauge, and as a consequence the Wannier functions are not uniquely determined. In a computer program, the phase of a Bloch function is simply that resulting from the diagonalisation routine used to solve the Fock equation, which is in practice arbitrary. The FT of rapidly oscillating phases across the  $k$ -point grid results in Wannier functions delocalised across the supercell. Wannier functions properly localised at one unit cell can be obtained by fixing the gauge of the Bloch functions relative to each other so that variations with  $\mathbf{k}$  are gradual. The natural gauge is that where the scalar product between the coefficients of the Bloch function at each  $\mathbf{k}$  and the  $\Gamma$ -point  $\mathbf{o}$  is real. Bloch functions in their natural gauge  $|p_{\mathbf{k}}^{\mathbf{n}}\rangle$  can be obtained from those with a random gauge  $|p_{\mathbf{k}}^{\mathbf{r}}\rangle$  straightforwardly

$$\sum_{\mu_1} C_{\mu_1}^{p_{\mathbf{o}}} C_{\mu_1}^{p_{\mathbf{k}}} = R e^{i\theta_p^{\mathbf{o}\mathbf{k}}} \quad (17)$$

$$|p_{\mathbf{k}}^{\mathbf{n}}\rangle = e^{-i\theta_p^{\mathbf{o}\mathbf{k}}} |p_{\mathbf{k}}^{\mathbf{r}}\rangle \quad (18)$$

Wannier functions can be further localised by rotating the Bloch functions  $p$  for a given  $\mathbf{k}$  among themselves before wannierisation. In particular, due to the invariance of the HF wavefunction, we are free to rotate the occupied bands among themselves to obtain highly localised occupied Wannier functions by maximising a chosen locality metric. To obtain a good initial guess for the optimisation routines, we construct diabatic Wannier functions. First, the Bloch orbitals of the  $\Gamma$ -point are localised by orthogonal transformation.

$$|i_{\mathbf{o}}\rangle = \sum_j |j_{\mathbf{o}}\rangle O_{ji} \quad (19)$$

The Bloch orbitals of the remaining  $k$ -points are chosen to be those with maximal similarity with the  $\Gamma$ -point. The locality of the orbitals of the  $\Gamma$ -point is thus transferred diabatically across the first Brillouin zone. The

unitary matrix that transforms the unlocalised Bloch orbitals at  $\mathbf{k}$  to those that best match  $\mathbf{0}$  is obtained through a single value decomposition of the similarity metric  $\mathbf{S}_{i_0}^{j\mathbf{k}} = \sum_{\mu_1} C_{\mu_1}^{i_0} C_{\mu_1}^{j\mathbf{k}}$

$$|i_{\mathbf{k}}\rangle = \sum_{jj'} |j_{\mathbf{k}}\rangle U_{jj'} V_{j'i} \quad (20)$$

$$\mathbf{S}_0^{\mathbf{k}} = \mathbf{U}\Sigma\mathbf{V} \quad (21)$$

In this work, we employ a convenient approximate localisation procedure for the Bloch orbitals of the  $\Gamma$ -point, where we simply replace them with the Choleski vectors of the  $\Gamma$ -point density. In this way, well-localised Wannier functions can be obtained through linear algebra without any expensive optimisation steps.

## B. IBO Wannier Functions

Well-localised Wannier functions have previously been obtained by optimising the Boy's metric<sup>81–84</sup>, or by generalised Pipek–Mezey metrics<sup>85–87</sup>. In this work we obtain well-localised Wannier functions by optimising the periodic generalisation of Knizia's intrinsic bond orbitals (IBOs),<sup>88</sup> which are constructed via intrinsic Bloch atomic orbitals (IAOs)  $\tau_i, \sigma_{\mathbf{m}}$ . As discussed in detail in Ref.<sup>80</sup>, our chosen PM locality metric is given by

$$\langle O \rangle_{\text{PM}} = \sum_{A_1, i_0} |Q_{i_0}^{A_1}|^4 = \sum_{A_1, i_0} \langle i_0 | \hat{P}_{A_1}^{\text{IAO}} | i_0 \rangle^4, \quad (22)$$

where

$$\hat{P}_{A_1}^{\text{IAO}} = \sum_{\tau \in A} \sum_{\sigma_{\mathbf{m}}} |\tau_i\rangle (S^{-1})_{\tau_i}^{\sigma_{\mathbf{m}}} \langle \sigma_{\mathbf{m}}|. \quad (23)$$

and the projector  $\hat{P}_{A_1}^{\text{IAO}}$  involves a restricted summation over the Bloch-IAOs belonging to the atom  $A$  and  $S_{\tau_i}^{\sigma_{\mathbf{m}}} = \langle \tau_i | \sigma_{\mathbf{m}} \rangle$ . Localization of the WFs is greatly aided by our diabatic Wannierisation procedure, which serves as an initial guess by fixing the gauge of the orbitals to vary smoothly with the Bloch functions at the  $\Gamma$ -point. Full implementation details, including the optimization algorithm and the explicit construction of the Bloch IAOs can be found in Ref.<sup>80</sup>. The IBO Wannier functions obtained via Bloch IAOs retain the same advantages as molecular IBOs, namely that they form chemically interpretable well-localised orbitals with a well-defined basis set limit and rapidly decaying orthogonality tails.

## IV. PNOS WITH PERIODIC BOUNDARY CONDITIONS

In the domain-based PNO approach, the MP2 amplitudes for pair  $i_0 j_1$  are expanded in a basis of PNOS  $\{\tilde{a}_{i_0 j_1}\}$ , which are specific to that pair

$$E^{i_0 j_1} = \sum_{\tilde{a}\tilde{b} \in [i_0 j_1]} (2g_{\tilde{a}\tilde{b}}^{i_0 j_1} - g_{\tilde{b}\tilde{a}}^{i_0 j_1}) t_{\tilde{a}\tilde{b}}^{i_0 j_1}. \quad (24)$$

In turn, the PNOS  $\tilde{a}_{i_0 j_1}$  are expanded in a domain of BvK PAOs  $\{\tilde{\mu}_1\}$  which is also specific to that pair

$$|\tilde{a}_{i_0 j_1}\rangle = \sum_{\mu_{\mathbf{m}} \in \mathcal{D}_{i_0 j_1}} |\tilde{\mu}_{\mathbf{m}}\rangle C_{\mu_{\mathbf{m}}}^{a, i_0 j_1}. \quad (25)$$

Our approach to constructing the PNOS  $\tilde{a}_{i_0 j_1}$  for the periodic case mirrors the approach we use for the molecular case.<sup>43,89</sup> First, we determine a domain of PAOs for each occupied orbital  $|i_1\rangle$  based on integral screening thresholds. Within this domain, we truncate the virtual space for each  $|i_1\rangle$  to the domain of PAOs  $\mathcal{D}_{i_1}$  and set of OSVs  $\{\tilde{a}_{i_1}\}$  that contribute above a threshold to the external MP2 density for pair  $|i_1 i_1\rangle$ . We use numerical Laplace integration and local density fitting to approximate the MP2 density for OSVs. These PAO and OSV spaces are merged to pair PAO domains and pair orbital sets, within which we construct a MP2 pair density using the semi-canonical approximation. The virtual space for each pair  $|i_0 j_1\rangle$  is then finally truncated to the domain of PAOs  $\mathcal{D}_{i_0 j_1}$  and set of PNOS  $\{\tilde{a}_{i_0 j_1}\}$  that contribute to the external MP2 density for pair  $|i_0 j_1\rangle$  above a threshold. For the molecular case, the appropriate truncation threshold at each step has been carefully characterised and linked to the overall PNO truncation threshold  $T_{\text{PNO}}$  and we use these thresholds without modification. In the following, we give the details of the generalisation of PAOs, OSVs, PNOS and local density fitting to include periodic boundary conditions.

### A. BvK PAOs

The BvK PAOs are the projection of the BvK AO onto the space spanned by the virtual Wannier orbitals  $a_1$

$$|\tilde{\mu}_0\rangle = \sum_{a_1} |a_1\rangle \langle a_1 | \mu_0 \rangle_{\text{BvK}} = \sum_{\nu_{\mathbf{m}}} |\nu_{\mathbf{m}}\rangle \hat{C}_{\nu_{\mathbf{m}}}^{\mu_0} \quad (26)$$

$$\hat{C}_{\nu_{\mathbf{m}}}^{\mu_0} = \sum_{a_1 \kappa_{\mathbf{n}}} C_{\nu_{\mathbf{m}}}^{a_1} C_{\kappa_{\mathbf{n}}}^{a_1} S_{\mu_0}^{\kappa_{\mathbf{n}}} \quad (27)$$

$$S_{\mu_0}^{\kappa_{\mathbf{n}}} = \langle \mu_0 | \kappa_{\mathbf{n}} \rangle_{\text{BvK}} = \sum_{\mathbf{N}} \langle \mu_0 | \kappa_{\mathbf{n}+\mathbf{N}} \rangle \quad (28)$$

Since the Wannier functions and BvK AOs are all translational copies of the corresponding functions in the reference cell  $\mathbf{0}$ , the PAOs also inherit translational symmetry  $\hat{C}_{\nu_{\mathbf{m}}}^{\mu_1} = \hat{C}_{\nu_{\mathbf{m}-1}}^{\mu_0}$ . The overlap of the BvK AO functions within the BvK cell is evaluated as a sum over regular overlap integrals for the infinite periodic images of the individual AOs. The transformation coefficients  $\tilde{C}_{\nu_{\mathbf{m}}}^{\mu_1}$  for the contravariant PAOs  $|\hat{\mu}_1\rangle$  are the right-hand Moore–Penrose pseudo inverse of  $\hat{C}_{\nu_{\mathbf{m}}}^{\mu_1}$ .<sup>89</sup> Our approach to forming OSVs employs a numerical Laplace transformation and we require Laplace transformed BvK PAOs. These



are defined as

$$|\tilde{\mu}_0^z\rangle = \sum_{\mathbf{a}_k} |a_k\rangle e^{-(\epsilon_{a_k} - \epsilon_F)t_z} \langle a_k | \tilde{\mu}_0 \rangle_{\text{BvK}} \quad (29)$$

$$= \sum_{\nu_m} |\nu_m\rangle \hat{C}_{\nu_m}^{\mu_0, z} \quad (30)$$

$$\hat{C}_{\nu_m}^{\mu_0, z} = \sum_{a n n' \kappa_m} C_{\nu_m}^{a n'} L_{n' n}^{a, z} C_{\kappa_1}^{a n} S_{\mu_0}^{\kappa_1} \quad (31)$$

$$L_{n' n}^{a, z} = \sum_{\mathbf{k}} (V_{n'}^{\mathbf{k}})^* e^{-(\epsilon_{a_k} - \epsilon_F)t_z} V_n^{\mathbf{k}} \quad (32)$$

where  $\epsilon_F$  is the Fermi level and  $t_z$  is a Laplace integration grid point. The Laplace transformed PAOs  $|\tilde{\mu}_1^z\rangle$  are also all translational copies of  $|\tilde{\mu}_0^z\rangle$ .

### B. OSVs

Orbital specific virtuals are PNOs for diagonal pairs  $|i_1 i_1\rangle$ . Our approach is to closely follow the molecular PNO-MP2 implementation and to obtain OSVs as an intermediary for the purpose of accelerating the determination of PNOs. We obtain OSVs for each orbital  $|i_1\rangle$  as eigenvectors of an approximate external density matrix for pair  $|i_1 i_1\rangle$ , which we construct in a principal domain of PAOs  $\tilde{\mu} \in \mathcal{D}_{i_1}$  selected using the greedy algorithm described in Ref. 89. The external density is computed from first-order amplitudes for diagonal pairs approximated using a numerical Laplace transformation.<sup>43,90,91</sup> The integration points  $z$  and weights  $w_z$  are determined from the orbital eigenvalues of the supercell in the same way as for molecular calculations. It is only necessary to compute the OSVs for the reference cell, since those for the other cells can be obtained through translational symmetry. Specifically, the OSV coefficients  $C_{\nu_m}^{\tilde{\mu}}$  and occupation numbers  $n_{\tilde{a}}$  for orbital  $i_0$  are obtained via

$$t_{\tilde{\mu}_1 \tilde{\kappa}_n}^{i_0 i_0} = \sum_z w_z \langle \tilde{\mu}_1^z \tilde{\kappa}_n^z | i_0^z i_0^z \rangle_{\text{BvK}} \quad (33)$$

$$D_{\tilde{\mu}_1}^{\tilde{\nu}_m} = \sum_{\kappa_n} 4 t_{\tilde{\mu}_1 \tilde{\kappa}_n}^{i_0 i_0} t_{\tilde{\nu}_m \tilde{\kappa}_n}^{i_0 i_0} \quad (34)$$

$$\sum_{\nu_m} D_{\tilde{\mu}_1}^{\tilde{\nu}_m} C_{\tilde{\nu}_m}^{\tilde{\mu}} = \sum_{\nu_m} S_{\tilde{\mu}_1}^{\tilde{\nu}_m} C_{\tilde{\nu}_m}^{\tilde{\mu}} n_{\tilde{a}} \quad (35)$$

Here  $S_{\tilde{\mu}}^{\tilde{\nu}}$  is the overlap between the selected PAOs  $S_{\tilde{\mu}_1}^{\tilde{\nu}_m} = \langle \tilde{\mu}_1 | \tilde{\nu}_m \rangle_{\text{BvK}}$  and  $C_{\tilde{\nu}_m}^{\tilde{\mu}}$  are the transformation coefficients from the PAOs to the OSVs  $|\tilde{a}_{i_0}\rangle$ , which are particular to each orbital  $|i_0\rangle$ . Only those OSVs  $\{\tilde{a}_{i_0}\}$  with occupation numbers  $n_{\tilde{a}}$  greater than a user defined threshold are retained. The OSVs for  $|i_1\rangle$  are simply  $C_{\tilde{\nu}_{m+1}}^{\tilde{\mu}}$ , obtained from those of  $|i_0\rangle$  by translation.

Once the OSVs are determined, the OSV-SOS-MP2 energy can be used to compute approximate pair energies for the purpose of discarding insignificant pairs and providing an estimate of their contribution to the total

energy

$$E_{\text{SOS}}^{i_0 j_1} = - \sum_{\tilde{a} \in [i_0], \tilde{b} \in [j_1]} \frac{g_{\tilde{a}\tilde{b}}^{i_0 j_1} g_{\tilde{a}\tilde{b}}^{i_0 j_1}}{\epsilon_{\tilde{a}} + \epsilon_{\tilde{b}} - f_{i_0}^{i_0} - f_{j_1}^{j_1}}. \quad (36)$$

The OSV-SOS-MP2 energy does not contain exchange contributions and can be evaluated efficiently using asymmetric density fitting.

### C. PNOs

Having obtained PAO domains and OSVs for every orbital  $|i_1\rangle$ , we construct initial PAO pair domains  $\mathcal{D}_{i_0 j_1}$  and pair specific virtuals  $\{\tilde{a}_{i_0 j_1}\}$  for each pair  $|i_0 j_1\rangle$  by merging the respective PAO and OSV domains for  $|i_0\rangle$  and  $|j_1\rangle$ . We then form PNOs for each pair as eigenvectors of an approximate external density matrix constructed within this pair specific subspace. The external density is computed from first-order amplitudes using the semi-canonical approximation, where the pair specific orbitals are canonicalised to diagonalise the virtual block of the Fock matrix for each pair  $f_{\tilde{a}}^{\tilde{b}} = \epsilon_{\tilde{a}} \delta_{\tilde{a}\tilde{b}}$  and off-diagonal occupied Fock matrix elements are neglected.

$$t_{\tilde{a}\tilde{b}}^{i_0 j_1} = -(\epsilon_{\tilde{a}} - \epsilon_{\tilde{b}} - f_{i_0}^{i_0} - f_{j_1}^{j_1})^{-1} g_{\tilde{a}\tilde{b}}^{i_0 j_1} \quad (37)$$

$$u_{\tilde{a}\tilde{b}}^{i_0 j_1} = 2t_{\tilde{a}\tilde{b}}^{i_0 j_1} - t_{\tilde{b}\tilde{a}}^{i_0 j_1} \quad (38)$$

$$D_{\tilde{a}}^{\tilde{b}} = 2 \sum_{\tilde{c}} (t_{\tilde{a}\tilde{c}}^{i_0 j_1} u_{\tilde{b}\tilde{c}}^{i_0 j_1} + t_{\tilde{c}\tilde{a}}^{i_0 j_1} u_{\tilde{c}\tilde{b}}^{i_0 j_1}) \quad (39)$$

$$D_{\tilde{a}}^{\tilde{b}} C_{\tilde{b}}^{\tilde{a}} = n_{\tilde{a}} C_{\tilde{a}}^{\tilde{a}} \quad (40)$$

Optionally, a further truncation of the PAO domains to principle pair domains can be performed prior to finding the eigenvectors of the external pair density matrix. The final space of retained PNOs are those with occupation numbers greater than the user defined PNO threshold  $n_{\tilde{a}} > T_{\text{PNO}}$  and the fully coupled first-order amplitude equations are solved in this subspace. Since the PNOs and corresponding integrals and amplitudes for pairs  $|i_1 j_m\rangle$  are translational copies of  $|i_0 j_1\rangle$ , it is only necessary to compute and store those for  $|i_0 j_1\rangle$ .

PNO-MP2 energy under the semi-canonical approximation (PNO-SC-MP2) can be computed as a byproduct of forming PNOs.

$$E_{\text{SC}}^{i_0 j_1} = \sum_{\tilde{a}\tilde{b} \in [i_0 j_1]} u_{\tilde{a}\tilde{b}}^{i_0 j_1} g_{\tilde{a}\tilde{b}}^{i_0 j_1} \quad (41)$$

The difference between the PNO-SC-MP2 energy before and after truncation of the PNO space to  $\{\tilde{a}_{i_0 j_1}\}$  provides an estimate for the contribution of the discarded PNOs to the total energy.

## V. PNO-MP2 WITH PERIODIC BOUNDARY CONDITIONS

The final amplitude equations for periodic PNO-MP2 are analogous to those of non-periodic PNO-MP2.

$$\begin{aligned}
0 = & g_{\tilde{a}\tilde{b}}^{i_0j_1} + (\varepsilon_{\tilde{a}} + \varepsilon_{\tilde{b}}) t_{\tilde{a}\tilde{b}}^{i_0j_1} \\
& - \sum_{k_m} \sum_{\tilde{c}\tilde{d} \in [k_mj_1]} S_{\tilde{a},i_0j_1}^{\tilde{c},k_mj_1} S_{\tilde{b},i_0j_1}^{\tilde{d},k_mj_1} t_{\tilde{c}\tilde{d}}^{k_mj_1} f_{k_m}^{i_0} \\
& - \sum_{k_m} \sum_{\tilde{c}\tilde{d} \in [i_0k_m]} S_{\tilde{a},i_0j_1}^{\tilde{c},i_0k_m} S_{\tilde{b},i_0j_1}^{\tilde{d},i_0k_m} t_{\tilde{c}\tilde{d}}^{i_0k_m} f_{k_m}^{j_1} \quad (42)
\end{aligned}$$

where  $\tilde{a}\tilde{b} \in [i_0j_1]$  and  $S_{\tilde{a},i_0j_1}^{\tilde{c},k_mj_1}$  is the overlap between PNOs for pair  $i_0j_1$  and pair  $k_mj_1$ . The amplitude equations are solved iteratively for every pair  $|i_0j_1\rangle$  and the correlation energy per unit cell is then evaluated as

$$E_{\text{corr}} = \frac{2}{1 + \delta_{i_0j_1}} \sum_{i_0 \leq j_1} \sum_{\tilde{a}\tilde{b} \in [i_0j_1]} (2g_{\tilde{a}\tilde{b}}^{i_0j_1} - g_{\tilde{b}\tilde{a}}^{i_0j_1}) t_{\tilde{a}\tilde{b}}^{i_0j_1} + \Delta \quad (43)$$

where  $\Delta$  is the correction term composed of the energy estimates for the discarded pairs and PNOs.

Since the WFs and PNO domains are rigorously translationally symmetric, the amplitudes, overlaps and Fock matrix elements spanning the entire supercell can be generated from the translationally unique set of objects where at least one index resides in the reference cell. For example,  $f_{k_m}^{j_1} = f_{k_m-1}^{j_0}$  and  $t_{\tilde{c}\tilde{d}}^{k_mj_1} = t_{\tilde{c}\tilde{d}}^{k_0j_1-m}$ , where it is understood that modulo arithmetic is applied to the lattice vectors.

## VI. PERIODIC LOCAL DENSITY FITTING

PNO methods require two-electron integrals in a different virtual basis for every pair, which introduces prohibitively high costs unless the density fitting approximation is invoked to reduce the expense of the integral transformation.<sup>92,93</sup> Density fitting also reduces the cost of the periodic image summation, since summation is only applied to two- and three-center integrals rather than to four-center integrals.

Local density fitting approximates the ERI between two charge densities  $\rho^A(\mathbf{r}_1)$  and  $\rho^B(\mathbf{r}_2)$  as

$$(\rho^A|\rho^B)_{\text{BvK}} \approx \sum_{P_m \in \mathcal{D}_A} \sum_{Q_l \in \mathcal{D}_B} C_{P_m}^A V_{P_m Q_l} C_{Q_l}^B \quad (44)$$

$$V_{P_m Q_l} = (P_m|Q_l)_{\text{BvK}} = \sum_{\mathbf{L}} (\tilde{P}_m|\tilde{Q}_{l+\mathbf{L}}) \quad (45)$$

$$C_{P_m}^A = \sum_{Q_l \in \mathcal{D}_A} \gamma_{Q_l}^A V_{P_m Q_l}^{-1} \quad (46)$$

$$\gamma_{Q_l}^A = (\rho^A|Q_l)_{\text{BvK}} = \sum_{\mathbf{L}} (\tilde{\rho}^A|\tilde{Q}_{l+\mathbf{L}}) \quad (47)$$

Here  $\tilde{\rho}$  is the charge density arising from the individual AOs within the BvK supercell, without image contributions, and, similarly,  $\tilde{Q}$  are individual DF functions. In DLPNO-MP2, the relevant charge densities are  $\rho = i_1\tilde{a}$ . For the SOS-MP2 energy estimates, asymmetric density fitting is used,<sup>94</sup> where the density fitting domains are local to  $A$  or  $B$ , but for all other integrals the usual robust formulation is used,<sup>95</sup> where  $\mathcal{D}_A = \mathcal{D}_B$  and the equations simplify to  $\gamma^A \mathbf{V}^{-1} \gamma^B$ .

To apply density fitting in periodic calculations, consideration must be given to the convergence of the lattice summations over periodic images for the two- and three-center integrals  $\mathbf{V}$  and  $\gamma$ .

### A. Coulomb lattice summation

The Coulomb interaction between a charge density  $\tilde{\rho}^A(\mathbf{r}_1)$  and an infinite lattice of charge densities  $\tilde{\rho}_L^B(\mathbf{r}_2)$  is not necessarily absolutely convergent, and for non-neutral charge densities, even divergent. This property manifests differently<sup>73,74,96</sup> in direct or reciprocal space representations and has profound implications for solid state simulations. A century after the seminal works by Born and von Kármán, Madelung, Ewald and others,<sup>66,67,97,98</sup> the appropriate treatment of periodic lattice sums in the context of efficient electronic structure theory remains an active research field.

Table II lists the convergence properties of lattice summations of the multipolar contributions to a charge distribution consisting of charges, dipoles, quadrupoles etc. which are denoted by  $s$ ,  $p$ ,  $d$ , etc. Since the relevant densities  $\rho = i_1\tilde{a}$  in MP2 are chargeless, divergent terms can be avoided through chargeless density fitting. The conditional convergence of the dipole-dipole terms in 3D arises from a residual surface energy, whose value depends on the shape of the surface of the lattice sum as it expands to infinity. To obtain the correct integrals, this surface energy must be removed.

The conditional convergence of dipole-dipole lattices has been investigated by many researchers. An instructive textbook example that illustrates the geometric nature of this effect is the Madelung constant of an NaCl. The cubic unit cell arrangement leads to a vanishing cell dipole moment, resulting in a fast absolutely convergent lattice sum, whereas the rhombohedral unit cell only yields the correct value if the surface effect due to the cell dipole moment is properly taken into account.<sup>99,100</sup> Of particular relevance to the current discussion are the numerous works in the context of LCAO-based Hartree-Fock,<sup>69,72,100,101</sup> and MP2,<sup>7,11,17,28</sup> periodic density fitting<sup>69-71</sup> and the multipole method.<sup>69,74,75,77,102-104</sup> In addition, see also Refs. 105-108 for a more general discussion on the nature of the surface effect.

TABLE II: Convergence properties of Coulomb lattice sums between multipole contributions to charge densities  $\sum_{\mathbf{L}}(\dot{\rho}^A|\dot{\rho}_{\mathbf{L}}^B)$ .

$(\rho^A \rho^B)$	Decay	1D	2D	3D
$(s s)$	$(r_{12})^{-1}$	divergent	divergent	divergent
$(s p)$	$(r_{12})^{-2}$	absolute	absolute	divergent
$(s d)$	$(r_{12})^{-3}$	absolute	absolute	conditional
$(p p)$	$(r_{12})^{-3}$	absolute	absolute	conditional
$(s f)$	$(r_{12})^{-4}$	absolute	absolute	absolute
$(p d)$	$(r_{12})^{-4}$	absolute	absolute	absolute

### B. Chargeless density fitting

To fit a chargeless density using local density fitting, we adapt the procedure outlaid by Burow *et al.*<sup>69,76</sup>. The linear combination of DF functions forming the approximate density can be resolved into a charged ( $\parallel$ ) and chargeless ( $\perp$ ) component

$$\sum_{Q_1} |\dot{Q}_1\rangle C_{Q_1} = \sum_{Q_1} |\dot{Q}_1\rangle C_{Q_1}^{\parallel} + \sum_{Q_1} |\dot{Q}_1\rangle C_{Q_1}^{\perp} \quad (48)$$

where

$$\mathbf{C}^{\perp} = \left( \mathbf{1} - \frac{\mathbf{n}\mathbf{n}^T}{|\mathbf{n}|^2} \right) \mathbf{C} = \mathbf{P}^{\perp} \mathbf{C} \quad (49)$$

$$n_{Q_1} = \int_{-\infty}^{\infty} \dot{Q}_1(\mathbf{r}) d^3\mathbf{r} \quad (50)$$

The vector  $\mathbf{n}$  is the linear combination of  $\dot{Q}_1$  that results in a charge and is specific to the local density fitting domain  $\mathcal{D}$ . To fit a chargeless density, the charged component of the fitting basis is projected out before solving for the fitting coefficients, which results in

$$(\rho^A|\rho^B)_{\text{BvK}} \approx \mathbf{C}_A^{\perp} \mathbf{V}^{\perp} \mathbf{C}_B^{\perp} \quad (51)$$

$$\mathbf{V}^{\perp} = \mathbf{P}_A^{\perp} \mathbf{V} \mathbf{P}_B^{\perp} \quad (52)$$

$$\mathbf{C}_A^{\perp} = \gamma_A^{\perp} (\mathbf{V}_A^{\perp})^{-1} \quad (53)$$

$$\gamma_A^{\perp} = \gamma_A \mathbf{P}_A^{\perp} \quad (54)$$

For robust DF, this simplifies to

$$(\rho^A|\rho^B)_{\text{BvK}} \approx \gamma_A^{\perp} (\mathbf{V}^{\perp})^{-1} \gamma_B^{\perp} \quad (55)$$

### C. Surface charge cancellation

The dipole of a charge density can be represented as a set of six point charges placed at the centers of the faces of the BvK supercell. Periodically repeating these dipoles within a finite volume  $\mathcal{M} = \mathcal{M}_a \mathcal{M}_b \mathcal{M}_c$  results in a cancellation of all point charges within the shape, but leaves uncanceled positive and negative charges on opposite faces. The electrostatic interaction of these charges

with the dipole of the charge density in the reference supercell gives rise to a surface energy that vanishes in 1D and 2D, but converges to a shape-dependent value as  $\mathcal{M}$  increases in 3D. The correct integrals for BvK boundary conditions are obtained from lattice summation protocols that impose ‘tin foil’<sup>107</sup> conditions at the surface, where there is no artificial surface contribution to the energy.

To eliminate the surface contribution, we follow the method by Stolarczyk and Piela,<sup>72</sup> which has been adapted to the LCAO Hartree–Fock method in `riper`<sup>69</sup> and described in detail in Ref. 76. To each auxiliary basis function in the lattice summation, we add the set of six point charges located at the faces of the BvK supercell within which the function resides, that exactly cancel the dipole of the function.

$$(P_{\mathbf{m}}|Q_1)_{\text{BvK}} = \sum_{\mathbf{L}} (\dot{P}_{\mathbf{m}}|\dot{Q}_{1+\mathbf{L}} + \dot{d}_{\mathbf{L}}^{Q_1}) \quad (56)$$

$$(\rho^A|Q_1)_{\text{BvK}} = \sum_{\mathbf{L}} (\dot{\rho}^A|\dot{Q}_{1+\mathbf{L}} + \dot{d}_{\mathbf{L}}^{Q_1}) \quad (57)$$

$$\dot{d}_{\mathbf{L}}^{Q_1}(\mathbf{r}) = \sum_{\mathbf{I}} q_{\mathbf{I}}^{Q_1} \delta(\mathbf{r} - \tfrac{1}{2}\mathbf{R}_{\mathbf{I}} - \mathbf{R}_{\mathbf{L}}) \quad (58)$$

Here  $\mathbf{I}$  are the unit BvK supercell displacements  $(\pm 1, 0, 0), (0, \pm 1, 0), (0, 0, \pm 1)$ . In one and two dimensional calculations,  $\mathbf{I}$  only includes the periodic lattice vectors, and two and four point charges are used, respectively, to cancel the dipole in the periodic degrees of freedom. A 2D case is illustrated in Fig. 2. The Cartesian dipole components of a function  $\dot{Q}_1$  are given by

$$p_{\alpha}^{Q_1} = - \int_{-\infty}^{\infty} \alpha \dot{Q}_1(\mathbf{r}) d^3\mathbf{r} \quad \alpha = x, y, z \quad (59)$$

where the minus is due to the electronic charge. The values of the point charges  $q_{\mathbf{I}}^{Q_1}$  that cancel the dipole are obtained by transforming  $\mathbf{p}^{Q_1}$  to the BvK lattice to obtain  $p_a^{Q_1}, p_b^{Q_1}, p_c^{Q_1}$ . The point charges that cancel the dipole in lattice vector  $a$ , placed at supercell displacements of  $(\pm 0.5, 0, 0)$ , are  $\mp p_a^{Q_1}/|\mathbf{A}|$ , and similarly for the other lattice vectors.

In our pilot implementation, we evaluate the integrals through direct space lattice summation without applying any fast multipole acceleration techniques.<sup>74,75,77</sup> The lattice summation is truncated at a sufficiently large vol-

ume  $\mathcal{M}$  and the integrals are evaluated as

$$(P_{\mathbf{m}}|Q_1)_{\text{BvK}} = \sum_{\mathbf{L}} (\dot{P}_{\mathbf{m}}|\dot{Q}_{1+\mathbf{L}}) + \sum_{\mathbf{I}} q_{\mathbf{I}}^{Q_1} S_{P_{\mathbf{m}}}^{\mathbf{I}} \quad (60)$$

$$S_{P_{\mathbf{m}}}^{\mathbf{I}} = \sum_{\mathbf{L} \in \mathcal{F}_{\mathbf{I}}} (\dot{P}_{\mathbf{m}}|\delta(\mathbf{r} - \frac{1}{2}\mathbf{R}_{\mathbf{I}} - \mathbf{R}_{\mathbf{L}})) \quad (61)$$

$$(\mu_{\mathbf{m}}\nu_{\mathbf{n}}|Q_1)_{\text{BvK}} = \sum_{\mathbf{L}\mathbf{N}} (\dot{\mu}_{\mathbf{m}}\dot{\nu}_{\mathbf{n}+\mathbf{N}}|\dot{Q}_{1+\mathbf{L}}) + \sum_{\mathbf{I}} q_{\mathbf{I}}^{Q_1} S_{\mu_{\mathbf{m}}\nu_{\mathbf{n}}}^{\mathbf{I}} \quad (62)$$

$$S_{\mu_{\mathbf{m}}\nu_{\mathbf{n}}}^{\mathbf{I}} = \sum_{\mathbf{L} \in \mathcal{F}_{\mathbf{I}}} \sum_{\mathbf{N}} (\dot{\mu}_{\mathbf{m}}\dot{\nu}_{\mathbf{n}+\mathbf{N}}|\delta(\mathbf{r} - \frac{1}{2}\mathbf{R}_{\mathbf{I}} - \mathbf{R}_{\mathbf{L}})) \quad (63)$$

Here  $\mathcal{F}_{\mathbf{I}}$  refers to the set of lattice vectors on the  $\mathbf{I}^{\text{th}}$  face of  $\mathcal{M}$ . The surface correction term only applies to  $s$ -type and  $p$ -type DF functions, since all other functions have a zero dipole. The net dipole arising from the  $s$ -type functions in the density fitting integrals is well defined because the net charge is projected out. For 1D and 2D calculations, the surface correction terms are analogously defined, but are only applied in the periodic directions. The summation over  $\mathbf{N}$  in the three-center integrals is rapidly convergent since the overlaps of  $\dot{\mu}_{\mathbf{m}}$  and  $\dot{\nu}_{\mathbf{n}+\mathbf{N}}$  decay exponentially. The summation over  $\mathbf{L}$  is polynomially decaying, with the degree of the polynomial depending on the basis functions and whether the calculation is 1D, 2D or 3D. In our calculations we monitor the convergence of the integrals and resulting energies with the lattice extent  $\mathcal{M}$  and our values are accurate to the significant figures reported.

The charge projection and surface correction terms significantly complicate the exploitation of translational symmetry to obtain computational savings. While the corrected integrals are translationally symmetric after charge projection, the individual contributions are not. In particular, the lattice summation range and correction terms for  $s$ -type DF functions must be evaluated with reference to a common origin to ensure that the surface term is properly eliminated. We therefore compute the full set of AO integrals and correction terms in the supercell using the centre of the supercell as the origin. Integral evaluation through naive lattice summation is currently the primary computational bottleneck. The scaling of this step with system size is the same as the molecular code, which is asymptotically  $\mathcal{O}(N)$  when the supercell is large enough for the local DF domain to saturate and screening to be effective.

One further subtlety in the integral evaluation is that the correction term breaks the symmetry of the Coulomb metric  $V_{P_{\mathbf{m}}Q_1}$ . Symmetry is restored in the limit of large  $\mathcal{M}$ . We therefore symmetrise  $V_{P_{\mathbf{m}}Q_1}$ , which we find accelerates convergence with lattice extent.

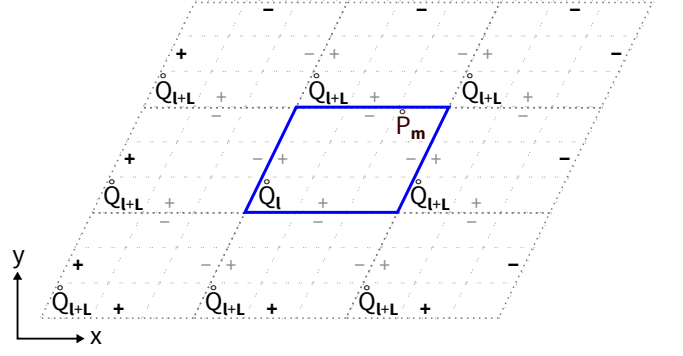


FIG. 2: Direct lattice summation for  $(P_{\mathbf{m}}|Q_1)_{\text{BvK}}$  with dipole correction.

## VII. COMPUTATIONAL DETAILS

Born–von Kármán domain-based local PNO-MP2 (BvK-DLPNO-MP2) has been implemented in a development version of the Turbomole program package within the `pnocsd` module, which has been used for all calculations presented here. Periodic LCAO-based Hartree–Fock with  $k$ -point sampling has recently become available in the `riper` module,<sup>69,77,109–111</sup> the output of which provides the Hartree–Fock Bloch functions and band energies required for MP2. The Bloch functions are localised for the ensuing correlation treatment through a new Wannier localization procedure which has been implemented into a development version of `riper`.<sup>80</sup>

All calculations utilize the pob-TZVP and pob-TZVP-rev2 basis sets which have specifically been optimized for LCAO simulations in the solid state.<sup>112,113</sup> For the density fitting, we use the def2-TZVP auxiliary basis in the Hartree–Fock<sup>114</sup> and MP2<sup>93</sup> calculations. Unless otherwise indicated, the frozen-core approximation is applied. DLPNO-MP2 calculations are performed for a series of increasingly accurate PNO thresholds ( $\mathcal{T}_{\text{PNO}} = 10^{-X}$ ,  $X = 6, 7, 8, 9$ ). Motivated by the observation that the largest discarded amplitude is proportional to the square of the PNO threshold, the complete PNO space (CPS) limit is estimated through a square root extrapolation using the two most accurate PNO energies.<sup>115,116</sup>

## VIII. RESULTS

To obtain reliable reference values for unit cell energies against which to test the performance of the BvK-DLPNO-MP2 method, we first leverage the molecular DLPNO<sup>43,89</sup> and canonical RI-MP2<sup>117</sup> infrastructure in Turbomole<sup>118,119</sup> to obtain unit cell energies through a molecular fragment approach. This enables us to assess the numerical stability of the BvK-DLPNO-MP2 method, to examine the rate of convergence to the thermodynamic limit, and to compare the relative accuracies of the HF and PNO approximations in the molecular and periodic settings. For future benchmarks, we provide ref-



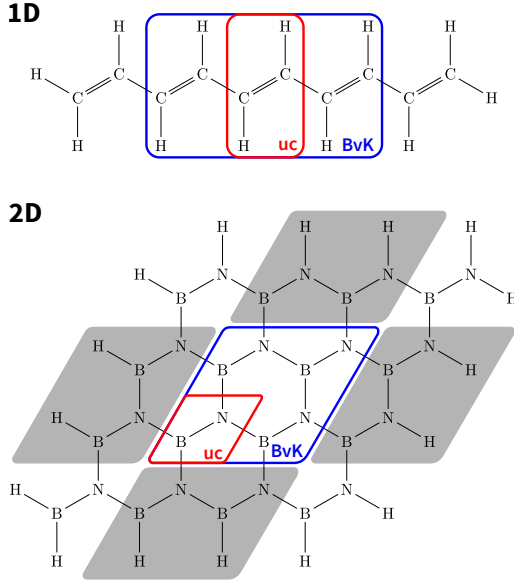


FIG. 3: Molecular cluster fragments that accommodate 1D and 2D BvK supercells (dotted box). The supercells of clusters with sum formula  $C_{2l}H_{2l+2}$  and  $B_{l^2}N_{l^2}H_{4l}$  are comprised of  $(l-2)$  and  $(l-2)^2$  unit cells (red box), respectively.

erence data using the BvK-DLPNO-MP2 method for various 2D and 3D systems.

#### A. Unit cell energies from molecular fragments

The molecular fragment method was used to obtain benchmark unit cell energies of 1D and 2D periodic systems. 3D examples were not possible due to the high computational expense of this approach. For 1D systems, we chose the linear alkene polymers  $C_2H_2$  and  $C_2HF$ , where in the latter the long-range dipole-dipole interactions due to the polar C–F bonds are expected to slow down the convergence with  $k$ -mesh. For 2D periodicity, we chose hexagonal boron nitride monolayers (lattice constant 2.501 Å; Ref. 120), which, unlike graphene, avoids Fermi-level degeneracies, ensuring stable periodic MP2 energies. The insulator is isoelectronic and structurally analogous to graphene but has a much higher band gap ( $\sim 6$  eV).<sup>121</sup> Unit cell geometries are deposited in the Supplementary Material.

In the molecular fragment approach, the energy of a unit cell is obtained by modeling the energy of a molecular fragment as a core of unit cells, plus contributions from faces, edges and corners. Starting from the periodic supercell structures, the fragments are generated by saturating the dangling bonds with hydrogens, as illustrated in Fig. 3. The energies of a series of increasing molecular fragments can then be used to subtract the surface contributions to obtain the correlation energy per unit cell, which converges to the thermodynamic limit as the size

of the molecular fragments increases.

For the 1D systems, the molecular energies of  $C_{2l}H_{2l+2}$  and  $C_{2l}H_{l+2}F_l$  are modeled as

$$E_{l,\text{tot}} = 2E_{\text{corner}} + (l-2)E_{\text{uc}}. \quad (64)$$

Using two fragment calculations, the corner energy can be subtracted to obtain an estimate of the unit cell energy

$$E_{\text{uc}}^{1D} = \frac{E_{l,\text{tot}} - E_{l-2,\text{tot}}}{2}. \quad (65)$$

The largest supercell size accommodated in the largest fragment corresponds to  $k_{\text{eff}} = (l-2)$ . For the 2D system, the total energy may be decomposed as

$$E_{l,\text{tot}} = 4E_{\text{corner}} + 4(l-2)E_{\text{edge}} + (l-2)^2E_{\text{uc}}. \quad (66)$$

To extract the unit cell energy for an effective mesh  $k_{\text{eff}}^2 = (l-2)^2$ , we now require three molecular clusters

$$E_{\text{uc}}^{2D} = \frac{E_{l,\text{tot}} - E_{l-2,\text{tot}} + E_{l-4,\text{tot}}}{8}. \quad (67)$$

The RI-HF, DLPNO-MP2 and canonical RI-MP2 correlation energies per unit cell obtained from this molecular fragment approach are listed in Table III. Inspection of the RI-HF data demonstrates the accuracy of the fragment approach. For all three systems, the HF energy converges to the thermodynamic limit obtained from periodic RI-HF calculations using *riper*, reported in the footnotes of Table III. As anticipated, the  $C_2HF$  convergence is much slower than that of  $C_2H_2$  and BN, which is attributed to the long range dipole-dipole interactions. A similar convergence behavior is observed for the DLPNO-MP2 correlation energies. All three systems display monotonic convergence to thermodynamic limit values for all PNO thresholds and for canonical RI-MP2. Moreover, it is encouraging that the extrapolated CPS correlation energies match the canonical values to within  $1 \times 10^{-5}$  Ha, demonstrating the accuracy and numerical stability of our PAO-OSV-PNO compression cascade. The final rows in Table III for each of the three systems provide the thermodynamic limit DLPNO-MP2 correlation energies for each PNO threshold. These values are accurate to  $1 \times 10^{-5}$  Ha.

#### B. Validating the Accuracy of BvK-DLPNO-MP2

Equipped with reference canonical MP2 unit cell energies at the thermodynamic limit for  $C_2H_2$ ,  $C_2HF$  and BN, we are now in a position to benchmark the BvK-DLPNO-MP2 method. The convergence with respect to the PNO threshold and supercell size for the BvK-DLPNO-MP2 correlation energies is displayed in Fig. 4, where we plot the deviation from the canonical thermodynamic limit. The BvK values are connected by solid lines and the corresponding molecular fragment data, which are included for comparison, by dotted lines.

TABLE III: Hartree–Fock and MP2 correlation energies per unit cell (in Hartree) extracted from molecular cluster energies.

effective $k$ -mesh	RI-HF <sup>a</sup>	PNO-RI-MP2					
		6	7	8	9	CPS	RI-MP2
1D C <sub>2</sub> H <sub>2</sub> (pob-TZVP)							
3	-76.88936	-0.27609	-0.27651	-0.27664	-0.27669	-0.27671	-0.27673
5	-76.88947	-0.27619	-0.27667	-0.27682	-0.27687	-0.27689	-0.27691
7	-76.88949	-0.27622	-0.27670	-0.27686	-0.27691	-0.27693	-0.27695
9	-76.88949	-0.27622	-0.27670	-0.27686	-0.27692	-0.27695	-0.27696
11	-76.88949	-0.27622	-0.27670	-0.27686	-0.27692	-0.27695	-0.27696
13	-76.88949	-0.27622	-0.27671	-0.27687	-0.27692	-0.27694	-0.27696
15	-76.88949	-0.27622	-0.27671	-0.27686	-0.27692	-0.27695	-0.27696
17	-76.88949	-0.27622	-0.27671	-0.27686	-0.27692	-0.27695	-0.27696
19	-76.88949	-0.27622	-0.27671	-0.27686	-0.27692	-0.27695	-0.27696
21	-76.88949	-0.27622	-0.27671	-0.27686	-0.27692	-0.27695	-0.27696
23	-76.88949	-0.27622	-0.27671	-0.27686	-0.27692	-0.27695	-0.27696
25	-76.88949	-0.27622	-0.27671	-0.27686	-0.27692	-0.27695	-0.27696
27	-76.88949	-0.27622	-0.27671	-0.27686	-0.27692	-0.27695	-0.27696
37	-76.88949	-0.27622	-0.27671	-0.27686	-0.27692	-0.27695	-0.27696
1D C <sub>2</sub> HF (pob-TZVP)							
3	-175.77440	-0.43895	-0.43978	-0.44006	-0.44016	-0.44021	-0.44022
5	-175.77476	-0.43873	-0.43958	-0.43988	-0.43999	-0.44004	-0.44005
7	-175.77496	-0.43850	-0.43936	-0.43967	-0.43979	-0.43985	-0.43985
9	-175.77508	-0.43831	-0.43921	-0.43953	-0.43964	-0.43969	-0.43970
11	-175.77516	-0.43824	-0.43912	-0.43943	-0.43955	-0.43961	-0.43961
13	-175.77521	-0.43812	-0.43906	-0.43938	-0.43949	-0.43954	-0.43955
15	-175.77524	-0.43808	-0.43903	-0.43934	-0.43945	-0.43950	-0.43951
17	-175.77526	-0.43811	-0.43900	-0.43931	-0.43943	-0.43949	-0.43949
19	-175.77527	-0.43810	-0.43899	-0.43930	-0.43941	-0.43946	-0.43947
21	-175.77528	-0.43809	-0.43897	-0.43929	-0.43940	-0.43945	-0.43946
23	-175.77529	-0.43806	-0.43897	-0.43928	-0.43939	-0.43944	-0.43946
25	-175.77530	-0.43807	-0.43896	-0.43928	-0.43939	-0.43944	-0.43945
27	-175.77530	-0.43805	-0.43896	-0.43927	-0.43938	-0.43943	-0.43945
37	-175.77531	-0.43805	-0.43895	-0.43926	-0.43938	-0.43944	-0.43944
2D BN (pob-TZVP-rev2)							
5 × 5	-79.29076	-0.21773	-0.21840	-0.21864	-0.21874	-0.21879	-0.21880
7 × 7	-79.29075	-0.21770	-0.21838	-0.21863	-0.21873	-0.21877	-0.21878
9 × 9	-79.29075	-0.21772	-0.21837	-0.21862	-0.21873	-0.21877	-0.21878
11 × 11	-79.29075	-0.21768	-0.21837	-0.21862	-0.21873	-0.21877	-0.21878

<sup>a</sup> Converged BvK-RI-HF energies: -76.88949 (C<sub>2</sub>H<sub>2</sub>), -175.77532 (C<sub>2</sub>HF), -75.29075 (BN).

We find that the molecular fragment and BvK-DLPNO-MP2 correlation energies converge to the same thermodynamic limit for each PNO threshold for all three examples tested. For C<sub>2</sub>H<sub>2</sub> and C<sub>2</sub>HF the agreement is to within 10<sup>-5</sup> Ha at  $k = 29$  and for BN the agreement is better than 10<sup>-4</sup> Ha at  $k = 11$ . The PNO approximation with BvK boundary conditions is therefore fully consistent with that of the molecular case, and the usual smooth convergence to the canonical limit is observed upon tightening the PNO threshold. Fig. 4 shows a striking difference in how the molecular and BvK energies approach the thermodynamic limit. For C<sub>2</sub>H<sub>2</sub> and BN, the molecular curves almost immediately plateau, whereas the BvK curves exhibit a slower convergence, necessitating comparably large supercells to achieve mHa accuracy.

To further examine the slow convergence, in Fig. 5 we plot the finite-size errors from BvK-DLPNO-MP2 and

molecular fragment DLPNO-MP2 ( $\mathcal{T}_{\text{PNO}} = 10^{-9}$ ) unit cell correlation energies together with the corresponding errors in the Hartree–Fock energy. The HF energy from the periodic calculations also displays a slower convergence to the thermodynamic limit compared to the fragment approach. These data indicate that the main source of the slow convergence of the BvK-DLPNO-MP2 correlation energy is most likely due to the finite-size errors in the underlying Hartree–Fock orbitals and band energies. Finite-size effects in the virtual HF orbitals and eigenvalues are not reflected in the HF energy, but have a direct impact on the MP2 correlation energy, which is the reason for the slow convergence of the BvK-DLPNO-MP2 energies for BN.

These findings are very interesting in the context of how the BvK-DLPNO-MP2 and Megacell-DLPNO-MP2 schemes (Paper II) approach the thermodynamic limit.

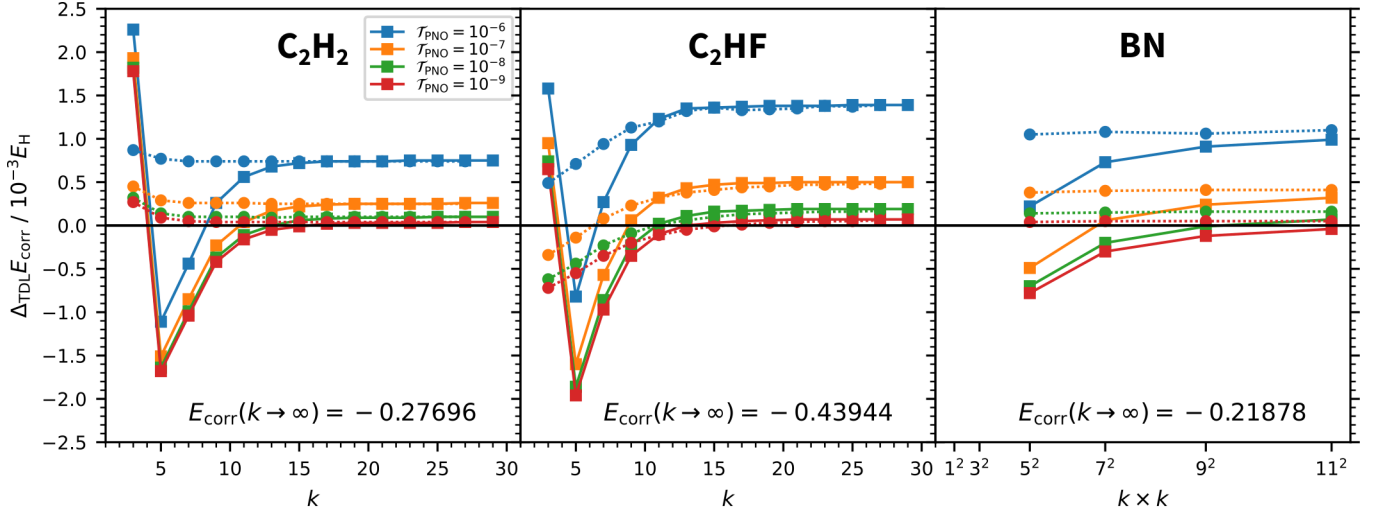


FIG. 4: Deviations from the canonical thermodynamic limit of periodic BvK-DLPNO-MP2 (solid) and fragment based DLPNO-MP2 (dashed) correlation energies per unit cell for  $\text{C}_2\text{H}_2$ ,  $\text{C}_2\text{HF}$  and a BN monolayer

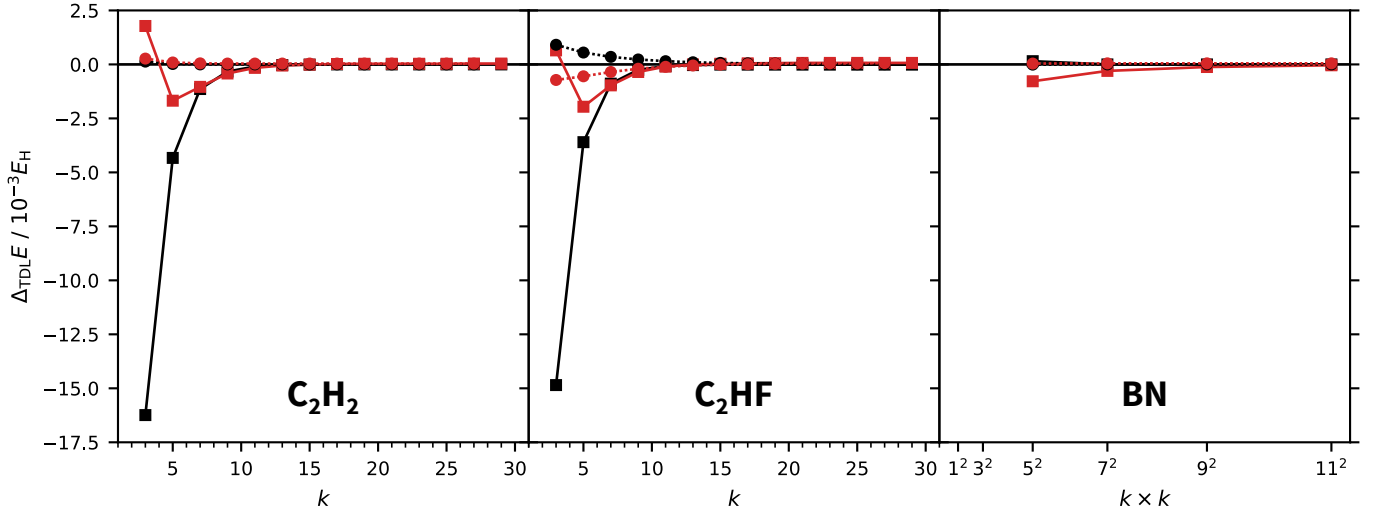


FIG. 5: Molecular (dash-dot) and periodic BvK (solid)  $T_{\text{PNO}} = 10^{-9}$  curves from Fig. 4 (red) juxtaposed with the convergence of the Hartree—Fock energy (black). The corresponding data are provided in the Supplementary Material.

The latter embeds the supercell for the correlation treatment in a larger megacell to ensure all WFs centered in the supercell are sufficiently decayed at the boundary of the megacell. Since the underlying HF calculation is for the larger megacell, the finite-size errors for this approach will be much smaller and we anticipate a more rapid convergence to the thermodynamic limit of the Megacell-DLPNO-MP2 correlation energy with respect to the supercell size.

Since an independent benchmark for a realistic 3D case using the molecular fragment approach was too expensive, we instead verify that the dipole correction scheme is correctly removing the surface energy by computing the correlation energy of the same lattice through two different unit cells. At the thermodynamic limit, these

calculations should yield the same HF and correlation energies. The results for cubic and rhombohedral LiH unit cells are reported in Table IV. Since the cubic cell contains four LiH units and the rhombohedral only one, the former energies are divided by four. The HF energies per LiH unit for the  $3 \times 3 \times 3$  cubic and  $5 \times 5 \times 5$  rhombohedral calculations agree to within 0.25 mHa, reducing to  $10^{-5}$  Ha for  $5 \times 5 \times 5$  and  $7 \times 7 \times 7$ . The DLPNO-MP2 correlation energies per LiH unit for the  $3 \times 3 \times 3$  cubic and  $5 \times 5 \times 5$  rhombohedral calculations agree to within 0.15 mHa, if the dipole correction is applied. If it is not, the energies deviate by 621 mHa. These data indicate that the implementation is correct. In Paper II of this series, we compare correlation energies computed using the BvK and Megacell schemes for 1D, 2D and 3D mate-

rials. We find that the correlation energies all converge to the same thermodynamic limit for each PNO threshold, providing further evidence that the level of accuracy of the PNO truncation scheme is entirely consistent for 1D, 2D and 3D, and molecular calculations.

TABLE IV: HF and BvK-DLPNO-MP2 ( $\mathcal{T}_{\text{PNO}} = 10^{-7}$ ) energies per LiH unit (Hartree) for a 3D LiH lattice with two different unit cells.

$k$ -mesh	Cubic		Rhombohedral	
	$3 \times 3 \times 3$	$5 \times 5 \times 5$	$5 \times 5 \times 5$	$7 \times 7 \times 7$
$n_{\text{atom}}$	216	1000	250	686
$E_{\text{HF}}$	-8.06035	-8.06058	-8.06060	-8.06059
$E_{\text{corr}}$				
... dip-cor	-0.03060		-0.03075	-0.03092
... no dip-cor	-0.077		-0.698	

### C. Illustrative 2D and 3D examples

To further demonstrate the capabilities of our current pilot BvK-DLPNO-MP2 implementation and provide reference data for future benchmarks, Table V shows DLPNO-MP2 unit cell energies for various 2D and 3D systems. All calculations were performed on a dual-socket workstation equipped with two Intel(R) Xeon(R) Gold 6248R CPUs (48 total cores), 386 GB of RAM and 1.8 TB disk within a few days of wall-time.

In addition to hexagonal BN (see also  $\mathcal{T}_{\text{PNO}} = 10^{-9}$  data in the Supplementary Material), we have computed the correlation energies for SiC and MoS<sub>2</sub> monolayers. SiC forms a planar honeycomb lattice but exhibits more polar bonds than BN. MoS<sub>2</sub> monolayers are promising candidates for future optoelectronic applications,<sup>124,125</sup> and form puckered honeycombs.<sup>126</sup> For monolayer MoS<sub>2</sub>, we were only able to obtain a full PNO series for a  $3 \times 3$  mesh whereas tight PNO thresholds for larger supercell sizes ran out of disk space. Since the current implementation does not yet make use of translational symmetry in the integral evaluation, three-center MO integrals over the whole BvK supercell must be stored on disk, which constitutes a significant bottleneck on our machines.

LiH and MgO both crystallize in the rock salt structure and have been benchmarked extensively in the context of LCAO-HF and MP2.<sup>78,127</sup> To diversify the benchmark set beyond materials, we also include hexagonal ice which is a prototypical example for hydrogen bonding, proton tunnelling and cooperativity in molecular crystals.<sup>128</sup> In all cases, the finite-size error can be reduced to within chemical accuracy except for monolayer MoS<sub>2</sub>, which emerges as a promising benchmark system.

## IX. CONCLUSION

Wavefunction-based many-body correlation theory provides a systematically improvable hierarchy of methods that can be used to independently verify and benchmark the accuracy of density functional predictions of electronic energies and properties of molecules and materials. The steep scaling of computational cost with system size presents a severe challenge when applying correlated wavefunction theories to periodic systems, where large simulation cells are required to capture all the relevant correlation lengthscales. We are therefore developing LCAO-based local correlation theory for periodic systems as a solution to this problem, at least for insulating materials. Domain-based pair natural orbital methods (DLPNO) have transformed the range of applicability of accurate coupled-cluster methods by using local approximations to reduce the cost to scale asymptotically only linearly with system size. The goal of our work is to develop the corresponding theory for periodic systems, where we aim to leverage large parts of the existing efficient molecular implementation in the Turbomole program package.

In this contribution, we have presented the periodic generalisation of DLPNO-MP2 theory using Born-von Kármán periodic boundary conditions. DLPNO-MP2 is the necessary first step towards DLPNO-CCSD(T) theory and DLPNO-CC3 theory for excited states. We have provided the complete set of equations for obtaining periodic PNOs for a pair of occupied Wannier functions, using periodic PAOs and OSVs as intermediaries via the PAO-OSV-PNO cascade. This work therefore generalises the earlier periodic PAO-based OSV-MP2 method introduced by Usvyat *et al.*<sup>30</sup>. The PNO approximations used are completely analogous to the molecular scheme and our calculations comparing unit cell energies computed from periodic calculations and molecular fragment calculations demonstrate that the PNO truncation errors are entirely equivalent. This makes it possible to straightforwardly combine results from molecular and periodic DLPNO calculations when studying molecular insertion in porous solids, or surface adsorption processes.

The primary difficulty for electronic structure methods under BvK conditions lies in the proper treatment of the infinite lattice sum of the electron repulsion integrals. We have used a chargeless local density fitting method that adds dipole-correction to cancel the surface energy and ensure convergent lattice sums for the two- and three-center ERIs. The method is numerically stable and the convergence with the extend of the lattice summation was sufficiently rapid that we could apply direct lattice summation without the aid of fast multipole techniques. Future incorporation of such methods would undoubtedly reduce the computational cost since the multipole lattice summation can be brought outside the loop over AOs. Integral evaluation is currently the main computational bottleneck of our current implementation. A scheme that uses maximises the use of translational symmetry for the

TABLE V: Benchmark frozen-core BvK-DLPNO-MP2 correlation energies, extrapolated to the complete PNO space (CPS) for various 2D (monolayer) and 3D materials. Unit cell geometries and XYZ coordinates are in the Supplementary Material.

		$k$ -mesh	BvK supercell		RI-HF	PNO-RI-MP2			
			basis func.	act. orb.		6	7	8	CPS
BN <sup>a</sup>	pob-TZVP-rev2	5×5	900	100	−79.29060	−0.21856	−0.21927	−0.21948	−0.21958
		7×7	1764	196	−79.29075	−0.21805	−0.21872	−0.21898	−0.21910
		9×9	2916	324	−79.29075	−0.21787	−0.21854	−0.21879	−0.21891
		11×11	4356	484	−79.29075	−0.21779	−0.21846	−0.21871	−0.21882
SiC <sup>b</sup>	pob-TZVP	3×3	360	36	−326.79555	−0.20004	−0.20044	−0.20058	−0.20065
		5×5	1000	100	−326.79905	−0.20101	−0.20180	−0.20202	−0.20212
		7×7	1960	196	−326.79928	−0.20089	−0.20171	−0.20202	−0.20216
		9×9	3240	324	−326.79929	−0.20086	−0.20164	−0.20193	−0.20206
		11×11	4840	484	−326.79929	−0.20081	−0.20161	−0.20189	−0.20203
MoS <sub>2</sub> <sup>c</sup>	pob-TZVP-rev2	3×3	711	108	−863.92030	−0.96718	−0.97253	−0.97477	
		5×5	1975	300	−863.92353	−0.93369	−0.94275		
		7×7	3871	588	−863.92352	−0.92956			
LiH <sup>d</sup>	pob-TZVP	5×5×5	1625	125	−8.06060	−0.03066	−0.03075	−0.03078	−0.03079
		7×7×7	4459	343	−8.06059	−0.03083	−0.03093	−0.03096	−0.03098
MgO <sup>e</sup>	pob-TZVP	3×3×3	999	108	−274.68268	−0.19631	−0.19651	−0.19660	−0.19664
		5×5×5	4625	500	−274.68452	−0.19853	−0.19882	−0.19896	−0.19902
MgO <sup>f</sup>	pob-TZVP	3×3×3	999	189	−274.68268	−0.25935	−0.25976	−0.25991	−0.25998
		5×5×5	4625	875	−274.68452	−0.26164	−0.26219	−0.26243	−0.26253
Ice <sup>g</sup>	pob-TZVP	3×3×3	3240	432	−304.26197	−0.74491	−0.74646	−0.74713	−0.74743

<sup>a</sup> Planar honeycomb, experimental lattice constant 2.501 Å.<sup>120</sup>

<sup>b</sup> Planar honeycomb, lattice constant 3.07 Å.<sup>120</sup>

<sup>c</sup> Puckered honeycomb, lattice constant 3.190 Å (Materials Project; mp-2815);<sup>122</sup> effective core potential for Mo.

<sup>d</sup> Rock salt type (rhombohedral), experimental cubic lattice constant 4.084 Å.<sup>123</sup>

<sup>e</sup> Rock salt type (rhombohedral), cubic lattice constant 4.339 Å; frozen Ne core for Mg.

<sup>f</sup> Frozen 1s<sup>2</sup>2s<sup>2</sup> core for Mg.

<sup>g</sup> Hexagonal ice (Materials Project; mp-697111).<sup>122</sup>

integrals to minimise the computational effort has yet to be worked out. Nevertheless, even with our pilot implementation, we were able to apply the BvK-DLPNO-MP2 method with a pob-TZVP basis to compute the correlation energies of 3D crystals of LiH, MgO and an ice polymorph, near the thermodynamic limit.

In paper II of this series,<sup>68</sup> we have presented an complementary strategy for treating crystalline materials, where supercell is embedded in a megacell, and rigorous translational symmetry is imposed for all Hamiltonian integrals and wavefunction parameters. This alternative approach avoids the complications arising from the lattice summation over periodic images in the integral evaluation. Encouragingly, we find that both schemes converge to the same thermodynamic limit for every PNO truncation threshold, underlining the stability of

the PNO local correlation approximations. A more detailed comparison of the relative merits of the two approaches will be the subject of future work.

## ACKNOWLEDGMENTS

We express our sincere thanks to Dr Denis Usvyat for providing benchmark thermodynamic limit MP2 energies computed using the CRYSCOR scheme. AN gratefully acknowledges funding through a Walter Benjamin Fellowship by the Deutsche Forschungsgemeinschaft (DFG, German Research Foundation) – 517466522. Financial support for AZ from the University of Oxford and Turbomole GmbH is gratefully acknowledged.

<sup>1</sup> Peter Kratzer and Jörg Neugebauer, “The basics of electronic structure theory for periodic systems,” *Front. Chem.* **7**, 106 (2019).

<sup>2</sup> R.M. Martin, *Electronic Structure: Basic Theory and Practical Methods*, 2nd ed. (Cambridge University Press, Cambridge, 2020).

<sup>3</sup> C. Pisani, M. Busso, G. Capecchi, S. Casassa, R. Dovesi, L. Maschio, C. Zicovich-Wilson, and M. Schütz, “Local-mp2 electron correlation method for nonconducting crystals,” *J. Chem. Phys.* **122**, 094113 (2005).

<sup>4</sup> Cesare Pisani, Martin Schütz, Silvia Casassa, Denis Usvyat, Lorenzo Maschio, Marco Lorenz, and



- Alessandro Erba, “Cryscor: a program for the post-hartree-fock treatment of periodic systems,” *Phys. Chem. Chem. Phys.* **14**, 7615–7628 (2012).
- <sup>5</sup> Mauro Del Ben, Jürg Hutter, and Joost VandeVondele, “Second-order møller-plesset perturbation theory in the condensed phase: An efficient and massively parallel gaussian and plane waves approach,” *J. Chem. Theory Comput.* **8**, 4177–4188 (2012).
  - <sup>6</sup> Tobias Schäfer, Benjamin Ramberger, and Georg Kresse, “Quartic scaling MP2 for solids: A highly parallelized algorithm in the plane wave basis,” *J. Chem. Phys.* **146**, 104101 (2017).
  - <sup>7</sup> Sylvia J. Bintrim, Timothy C. Berkelbach, and Hong-Zhou Ye, “Integral-direct hartree-fock and møller-Plesset perturbation theory for periodic systems with density fitting: Application to the benzene crystal,” *J. Chem. Theory Comput.* **18**, 5374–5381 (2022).
  - <sup>8</sup> Thomas Gruber, Ke Liao, Theodoros Tsatsoulis, Felix Hummel, and Andreas Grüneis, “Applying the coupled-cluster ansatz to solids and surfaces in the thermodynamic limit,” *Phys. Rev. X* **8**, 021043 (2018).
  - <sup>9</sup> Johanna P. Carbone, Andreas Irmeler, Alejandro Gallo, Tobias Schäfer, William Z. Van Benschoten, James J. Shepherd, and Andreas Grüneis, “CO adsorption on pt(111) studied by periodic coupled cluster theory,” *Faraday Discuss.* **254**, 586–597 (2024).
  - <sup>10</sup> Hong-Zhou Ye and Timothy C. Berkelbach, “Adsorption and vibrational spectroscopy of CO on the surface of MgO from periodic local coupled-cluster theory,” *Faraday Discuss.* **254**, 628–640 (2024).
  - <sup>11</sup> Lorenzo Maschio, Denis Usvyat, Frederick R. Manby, Silvia Casassa, Cesare Pisani, and Martin Schütz, “Fast local-MP2 method with density-fitting for crystals. I. theory and algorithms,” *Phys. Rev. B* **76**, 075101 (2007).
  - <sup>12</sup> Denis Usvyat, Lorenzo Maschio, Frederick R. Manby, Silvia Casassa, Martin Schütz, and Cesare Pisani, “Fast local-MP2 method with density-fitting for crystals. II. test calculations and application to the carbon dioxide crystal,” *Phys. Rev. B* **76**, 075102 (2007).
  - <sup>13</sup> James McClain, Qiming Sun, Garnet Kin-Lic Chan, and Timothy C. Berkelbach, “Gaussian-based coupled-cluster theory for the ground-state and band structure of solids,” *J. Chem. Theory Comput.* **13**, 1209–1218 (2017).
  - <sup>14</sup> So Hirata and Tomomi Shimazaki, “Fast second-order many-body perturbation method for extended systems,” *Phys. Rev. B* **80**, 085118 (2009).
  - <sup>15</sup> So Hirata, Rafał Podeszwa, Motoi Tobita, and Rodney J. Bartlett, “Coupled-cluster singles and doubles for extended systems,” *J. Chem. Phys.* **120**, 2581–2592 (2004).
  - <sup>16</sup> Idan Haritan, Xiao Wang, and Tamar Goldzak, “An efficient scaled opposite-spin MP2 method for periodic systems,” (2025), [arXiv:2503.20482 \[physics.chem-ph\]](https://arxiv.org/abs/2503.20482).
  - <sup>17</sup> Philippe Y. Ayala, Konstantin N. Kudin, and Gustavo E. Scuseria, “Atomic orbital Laplace-transformed second-order Møller-Plesset theory for periodic systems,” *J. Chem. Phys.* **115**, 9698–9707 (2001).
  - <sup>18</sup> Hong-Zhou Ye and Timothy C. Berkelbach, “Periodic local Coupled-Cluster theory for insulators and metals,” *J. Chem. Theory Comput.* **20**, 8948–8959 (2024).
  - <sup>19</sup> Michio Katouda and Shigeru Nagase, “Application of second-order møller-plesset perturbation theory with resolution-of-identity approximation to periodic systems,” *The Journal of Chemical Physics* **133**, 184103 (2010).
  - <sup>20</sup> George H Booth, Andreas Grüneis, Georg Kresse, and Ali Alavi, “Towards an exact description of electronic wavefunctions in real solids,” *Nature* **493**, 365–370 (2013).
  - <sup>21</sup> Igor Ying Zhang and Andreas Grüneis, “Coupled cluster theory in materials science,” *Front. Mater.* **6**, 123 (2019).
  - <sup>22</sup> Tamar Goldzak, Xiao Wang, Hong-Zhou Ye, and Timothy C. Berkelbach, “Accurate thermochemistry of covalent and ionic solids from spin-component-scaled MP2,” *J. Chem. Phys.* **157**, 174112 (2022).
  - <sup>23</sup> Andreas Grüneis, George H. Booth, Martijn Marsman, James Spencer, Ali Alavi, and Georg Kresse, “Natural orbitals for wave function based correlated calculations using a plane wave basis set,” *J. Chem. Theory Comput.* **7**, 2780–2785 (2011).
  - <sup>24</sup> Andreas Grüneis, “A coupled cluster and Møller-Plesset perturbation theory study of the pressure induced phase transition in the LiH crystal,” *J. Chem. Phys.* **143**, 102817 (2015).
  - <sup>25</sup> Benjamin X. Shi, Andrea Zen, Venkat Kapil, Péter R. Nagy, Andreas Grüneis, and Angelos Michaelides, “Many-body methods for surface chemistry come of age: Achieving consensus with experiments,” *J. Am. Chem. Soc.* **145**, 25372–25381 (2023).
  - <sup>26</sup> Theodoros Tsatsoulis, Felix Hummel, Denis Usvyat, Martin Schütz, George H. Booth, Simon S. Binnie, Michael J. Gillan, Dario Alfè, Angelos Michaelides, and Andreas Grüneis, “A comparison between quantum chemistry and quantum Monte Carlo techniques for the adsorption of water on the (001) LiH surface,” *J. Chem. Phys.* **146**, 204108 (2017).
  - <sup>27</sup> Maristella Alessio, Denis Usvyat, and Joachim Sauer, “Chemically accurate adsorption energies: CO and H<sub>2</sub>O on the MgO(001) surface,” *J. Chem. Theory Comput.* **15**, 1329–1344 (2019).
  - <sup>28</sup> Cesare Pisani, Lorenzo Maschio, Silvia Casassa, Migen Halo, Martin Schütz, and Denis Usvyat, “Periodic local MP2 method for the study of electronic correlation in crystals: Theory and preliminary applications,” *J. Comput. Chem.* **29**, 2113–2124 (2008).
  - <sup>29</sup> Denis Usvyat, “Linear-scaling explicitly correlated treatment of solids: Periodic local MP2-F12 method,” *J. Chem. Phys.* **139**, 194101 (2013).
  - <sup>30</sup> Denis Usvyat, Lorenzo Maschio, and Martin Schütz, “Periodic local MP2 method employing orbital specific virtuals,” *J. Chem. Phys.* **143**, 102805 (2015).
  - <sup>31</sup> S Saebø and P Pulay, “Local treatment of electron correlation,” *Annu. Rev. Phys. Chem.* **44**, 213–236 (1993).
  - <sup>32</sup> Jun Yang, Yuki Kurashige, Frederick R. Manby, and Garnet K. L. Chan, “Tensor factorizations of local second-order Møller-Plesset theory,” *J. Chem. Phys.* **134**, 044123 (2011).
  - <sup>33</sup> Zoltán Rolik and Mihály Kállay, “A general-order local coupled-cluster method based on the cluster-in-molecule approach,” *J. Chem. Phys.* **135**, 104111 (2011).
  - <sup>34</sup> Zoltán Rolik, Lóránt Szegedy, István Ladjánszki, Bence Ladóczki, and Mihály Kállay, “An efficient linear-scaling CCSD(T) method based on local natural orbitals,” *J. Chem. Phys.* **139**, 094105 (2013).
  - <sup>35</sup> Péter R. Nagy and Mihály Kállay, “Optimization of the linear-scaling local natural orbital CCSD(T) method: Redundancy-free triples correction using Laplace transform,” *J. Chem. Phys.* **146**, 214106 (2017).
  - <sup>36</sup> Péter R. Nagy, Gyula Samu, and Mihály Kállay, “Optimization of the linear-scaling lo-

- cal natural orbital CCSD(T) method: Improved algorithm and benchmark applications,” *J. Chem. Theory Comput.* **14**, 4193–4215 (2018).
- 37 Carsten Müller and Denis Usvyat, “Incrementally corrected periodic local MP2 calculations: I. the cohesive energy of molecular crystals,” *J. Chem. Theory Comput.* **9**, 5590–5598 (2013).
  - 38 Denis Usvyat, Keyarash Sadeghian, Lorenzo Maschio, and Martin Schütz, “Geometrical frustration of an argon monolayer adsorbed on the MgO (100) surface: An accurate periodic ab initio study,” *Phys. Rev. B* **86**, 045412 (2012).
  - 39 Thomas Mullan, Lorenzo Maschio, Peter Saalfraank, and Denis Usvyat, “Reaction barriers on non-conducting surfaces beyond periodic local MP2: Diffusion of hydrogen on  $\alpha$ -Al<sub>2</sub>O<sub>3</sub>(0001) as a test case,” *J. Chem. Phys.* **156**, 074109 (2022).
  - 40 Frank Neese, Andreas Hansen, and Dimitrios G. Liakos, “Efficient and accurate approximations to the local coupled cluster singles doubles method using a truncated pair natural orbital basis,” *J. Chem. Phys.* **131**, 064103 (2009).
  - 41 Christoph Riplinger and Frank Neese, “An efficient and near linear scaling pair natural orbital based local coupled cluster method,” *J. Chem. Phys.* **138**, 034106 (2013).
  - 42 Hans-Joachim Werner, Gerald Knizia, Christine Krause, Max Schwilk, and Mark Dornbach, “Scalable electron correlation methods I.: PNO-LMP2 with linear scaling in the molecular size and near-inverse-linear scaling in the number of processors,” *J. Chem. Theory Comput.* **11**, 484–507 (2015).
  - 43 Gunnar Schmitz, Benjamin Helmich, and Christof Hättig, “A ( $\mathcal{O}(N^3)$ ) scaling pno-mp2 method using a hybrid osv-pno approach with an iterative direct generation of osvs,” *Mol. Phys.* **111**, 2463–2476 (2013).
  - 44 Peter Pinski, Christoph Riplinger, Edward F. Valeev, and Frank Neese, “Sparse maps—a systematic infrastructure for reduced-scaling electronic structure methods. I. an efficient and simple linear scaling local MP2 method that uses an intermediate basis of pair natural orbitals,” *J. Chem. Phys.* **143**, 034108 (2015).
  - 45 David P. Tew and Christof Hättig, “Pair natural orbitals in explicitly correlated second-order möller–plesset theory,” *Int. J. Quantum Chem.* **113**, 224–229 (2013).
  - 46 Christof Hättig, David P. Tew, and Benjamin Helmich, “Local explicitly correlated second- and third-order Möller-Plesset perturbation theory with pair natural orbitals,” *J. Chem. Phys.* **136**, 204105 (2012).
  - 47 Christoph Riplinger, Barbara Sandhoefer, Andreas Hansen, and Frank Neese, “Natural triple excitations in local coupled cluster calculations with pair natural orbitals,” *J. Chem. Phys.* **139**, 134101 (2013).
  - 48 Yang Guo, Christoph Riplinger, Ute Becker, Dimitrios G. Liakos, Yury Minenkov, Luigi Cavallo, and Frank Neese, “Communication: An improved linear scaling perturbative triples correction for the domain based local pair-natural orbital based singles and doubles coupled cluster method [DLPNO-CCSD(T)],” *J. Chem. Phys.* **148**, 011101 (2018).
  - 49 Max Schwilk, Qianli Ma, Christoph Köppl, and Hans-Joachim Werner, “Scalable electron correlation methods. 3. efficient and accurate parallel local coupled cluster with pair natural orbitals (PNO-LCCSD),” *J. Chem. Theory Comput.* **13**, 3650–3675 (2017).
  - 50 Qianli Ma and Hans-Joachim Werner, “Scalable electron correlation methods. 5. parallel perturbative triples correction for explicitly correlated local coupled cluster with pair natural orbitals,” *J. Chem. Theory Comput.* **14**, 198–215 (2018).
  - 51 Gunnar Schmitz and Christof Hättig, “Accuracy of explicitly correlated local PNO-CCSD(T),” *J. Chem. Theory Comput.* **13**, 2623–2633 (2017).
  - 52 Gunnar Schmitz and Christof Hättig, “Perturbative triples correction for local pair natural orbital based explicitly correlated CCSD(F12\*) using laplace transformation techniques,” *J. Chem. Phys.* **145**, 234107 (2016).
  - 53 Dimitrios G. Liakos, Yang Guo, and Frank Neese, “Comprehensive benchmark results for the domain based local pair natural orbital coupled cluster method (DLPNO-CCSD(T)) for closed- and open-shell systems,” *J. Phys. Chem. A* **124**, 90–100 (2020).
  - 54 Masaaki Saitow, Ute Becker, Christoph Riplinger, Edward F. Valeev, and Frank Neese, “A new near-linear scaling, efficient and accurate, open-shell domain-based local pair natural orbital coupled cluster singles and doubles theory,” *J. Chem. Phys.* **146**, 164105 (2017).
  - 55 Christoph Riplinger, Peter Pinski, Ute Becker, Edward F. Valeev, and Frank Neese, “Sparse maps—a systematic infrastructure for reduced-scaling electronic structure methods. II. linear scaling domain based pair natural orbital coupled cluster theory,” *J. Chem. Phys.* **144**, 024109 (2016).
  - 56 Qianli Ma and Hans-Joachim Werner, “Scalable electron correlation methods. 2. parallel PNO-LMP2-F12 with near linear scaling in the molecular size,” *J. Chem. Theory Comput.* **11**, 5291–5304 (2015), pMID: 26574323.
  - 57 Gunnar Schmitz, Christof Hättig, and David P. Tew, “Explicitly correlated pno-mp2 and pno-ccsd and their application to the S66 set and large molecular systems,” *Phys. Chem. Chem. Phys.* **16**, 22167–22178 (2014).
  - 58 Qianli Ma, Max Schwilk, Christoph Köppl, and Hans-Joachim Werner, “Scalable electron correlation methods. 4. parallel explicitly correlated local coupled cluster with pair natural orbitals (PNO-LCCSD-F12),” *J. Chem. Theory Comput.* **13**, 4871–4896 (2017).
  - 59 David P. Tew, “Principal domains in F12 explicitly correlated theory,” in *New Electron Correlation Methods and their Applications, and Use of* Advances in Quantum Chemistry, Vol. 83, edited by Monika Musial and Philip E. Hoggan (Academic Press, 2021) pp. 83–106.
  - 60 Daniel Kats and Hans-Joachim Werner, “Multi-state local complete active space second-order perturbation theory using pair natural orbitals (PNO-MS-CASPT2),” *J. Chem. Phys.* **150**, 214107 (2019).
  - 61 Masaaki Saitow and Takeshi Yanai, “A multireference coupled-electron pair approximation combined with complete-active space perturbation theory in local pair-natural orbital framework,” *J. Chem. Phys.* **152**, 114111 (2020).
  - 62 Yang Guo, Kantharuban Sivalingam, Edward F. Valeev, and Frank Neese, “SparseMaps—a systematic infrastructure for reduced-scaling electronic structure methods. III. linear-scaling multireference domain-based pair natural orbital N-electron valence perturbation theory,” *J. Chem. Phys.* **144**, 094111 (2016).

- <sup>63</sup> Benjamin Helmich and Christof Hättig, “Local pair natural orbitals for excited states,” *J. Chem. Phys.* **135**, 214106 (2011).
- <sup>64</sup> Marius S. Frank and Christof Hättig, “A pair natural orbital based implementation of CCSD excitation energies within the framework of linear response theory,” *J. Chem. Phys.* **148**, 134102 (2018).
- <sup>65</sup> Achintya Kumar Dutta, Frank Neese, and Róbert Izsák, “Towards a pair natural orbital coupled cluster method for excited states,” *J. Chem. Phys.* **145**, 034102 (2016).
- <sup>66</sup> M. Born and T. von Kármán, “Über schwingungen in raumgittern,” *Phys. Z.* **13**, 297–309 (1912).
- <sup>67</sup> M. Born and T. von Kármán, “Zur theorie der spezifischen wärme,” *Phys. Z.* **14**, 15–19 (1913).
- <sup>68</sup> Andrew Zhu, Arman Nejad, Poramas Komonvasee, Kesha Sorathia, and David P. Tew, “Megacell-DLPNO-MP2 for periodic systems,” (2025), [arXiv:XXXX.XXXXX](https://arxiv.org/abs/XXXX.XXXXX).
- <sup>69</sup> Asbjörn M. Burow, Marek Sierka, and Fawzi Mohamed, “Resolution of identity approximation for the Coulomb term in molecular and periodic systems,” *J. Chem. Phys.* **131**, 214101 (2009).
- <sup>70</sup> Martin Schütz, Denis Usyat, Marco Lorenz, Cesare Pisani, Lorenzo Maschio, Silvia Casassa, and Migen Halo, “Density fitting for correlated calculations in periodic systems,” in *Accurate Condensed-Phase Quantum Chemistry*, edited by F. R. Manby (CRC Press, Boca Raton, 2010) pp. 29–55.
- <sup>71</sup> Hong-Zhou Ye and Timothy C. Berkelbach, “Fast periodic Gaussian density fitting by range separation,” *J. Chem. Phys.* **154**, 131104 (2021).
- <sup>72</sup> Leszek Z. Stolarczyk and Lucjan Piela, “Direct calculation of lattice sums. a method to account for the crystal field effects,” *Int. J. Quantum Chem.* **22**, 911–927 (1982).
- <sup>73</sup> G. Makov and M. C. Payne, “Periodic boundary conditions in *ab initio* calculations,” *Phys. Rev. B* **51**, 4014–4022 (1995).
- <sup>74</sup> Matt Challacombe, Chris White, and Martin Head-Gordon, “Periodic boundary conditions and the fast multipole method,” *J. Chem. Phys.* **107**, 10131–10140 (1997).
- <sup>75</sup> Konstantin N Kudin and Gustavo E Scuseria, “A fast multipole method for periodic systems with arbitrary unit cell geometries,” *Chem. Phys. Lett.* **283**, 61–68 (1998).
- <sup>76</sup> Asbjörn Manfred Burow, *Methoden zur Beschreibung von chemischen Strukturen beliebiger Dimensionalität mit der Dichtefunktionaltheorie unter periodischen Randbedingungen* (Universitätsbibliothek der Humboldt-Universität zu Berlin, Berlin, 2011) doi 10.18452/16415.
- <sup>77</sup> Roman Łazarski, Asbjörn M. Burow, and Marek Sierka, “Density functional theory for molecular and periodic systems using density fitting and continuous fast multipole methods,” *J. Chem. Theory Comput.* **11**, 3029–3041 (2015).
- <sup>78</sup> Andreas Irmeler, Asbjörn M. Burow, and Fabian Pauly, “Robust periodic Fock exchange with atom-centered Gaussian basis sets,” *J. Chem. Theory Comput.* **14**, 4567–4580 (2018).
- <sup>79</sup> Hendrik J. Monkhorst and James D. Pack, “Special points for Brillouin-zone integrations,” *Phys. Rev. B* **13**, 5188–5192 (1976).
- <sup>80</sup> Andrew Zhu and David P. Tew, “Wannier function localization using bloch intrinsic atomic orbitals,” *J. Phys. Chem. A* **128**, 8570–8579 (2024).
- <sup>81</sup> S. F. Boys, “Construction of some molecular orbitals to be approximately invariant for changes from one molecule to another,” *Rev. Mod. Phys.* **32**, 296–299 (1960).
- <sup>82</sup> J. M. Foster and S. F. Boys, “Canonical configurational interaction procedure,” *Rev. Mod. Phys.* **32**, 300–302 (1960).
- <sup>83</sup> Nicola Marzari and David Vanderbilt, “Maximally localized generalized wannier functions for composite energy bands,” *Phys. Rev. B* **56**, 12847–12865 (1997).
- <sup>84</sup> Giovanni Pizzi, Valerio Vitale, Ryotaro Arita, Stefan Blügel, Frank Freimuth, Guillaume Géranton, Marco Gibertini, Dominik Gresch, Charles Johnson, Takashi Koretsune, Julen Ibañez Azpiroz, Hyungjun Lee, Jae-Mo Lihm, Daniel Marchand, Antimo Marrazzo, Yuriy Mokrousov, Jamal I Mustafa, Yoshiro Nohara, Yusuke Nomura, Lorenzo Paulatto, Samuel Poncé, Thomas Ponweiser, Junfeng Qiao, Florian Thöle, Stepan S Tsirkin, Małgorzata Wierzbowska, Nicola Marzari, David Vanderbilt, Ivo Souza, Arash A Mostofi, and Jonathan R Yates, “Wannier90 as a community code: new features and applications,” *J. Phys.: Condens. Matter* **32**, 165902 (2020).
- <sup>85</sup> Elvar Ö. Jónsson, Susi Lehtola, Martti Puska, and Hannes Jónsson, “Theory and applications of generalized Pipek-Mezey Wannier functions,” *J. Chem. Theory Comput.* **13**, 460–474 (2017).
- <sup>86</sup> Marjory C. Clement, Xiao Wang, and Edward F. Valeev, “Robust Pipek-Mezey orbital localization in periodic solids,” *J. Chem. Theory Comput.* **17**, 7406–7415 (2021).
- <sup>87</sup> Lukas Schreder and Sandra Lubert, “Propagated (fragment) Pipek-Mezey Wannier functions in real-time time-dependent density functional theory,” *J. Chem. Phys.* **160**, 214117 (2024).
- <sup>88</sup> Gerald Knizia, “Intrinsic atomic orbitals: An unbiased bridge between quantum theory and chemical concepts,” *J. Chem. Theory Comput.* **9**, 4834–4843 (2013).
- <sup>89</sup> David P. Tew, “Principal domains in local correlation theory,” *J. Chem. Theory Comput.* **15**, 6597–6606 (2019).
- <sup>90</sup> Jan Almlöf, “Elimination of energy denominators in möller-plesset perturbation theory by a laplace transform approach,” *Chem. Phys. Lett.* **181**, 319–320 (1991).
- <sup>91</sup> Marco Häser and Jan Almlöf, “Laplace transform techniques in möller-plesset perturbation theory,” *J. Chem. Phys.* **96**, 489–494 (1992).
- <sup>92</sup> O. Vahtras, J. Almlöf, and M. W. Feyereisen, “Integral approximations for LCAO-SCF calculations,” *Chem. Phys. Lett.* **213**, 514–518 (1993).
- <sup>93</sup> Florian Weigend, Marco Häser, Holger Patzelt, and Reinhart Ahlrichs, “RI-MP2: optimized auxiliary basis sets and demonstration of efficiency,” *Chem. Phys. Lett.* **294**, 143–152 (1998).
- <sup>94</sup> David P. Tew, “Communication: Quasi-robust local density fitting,” *J. Chem. Phys.* **148**, 011102 (2018).
- <sup>95</sup> Brett I. Dunlap, “Robust and variational fitting,” *Phys. Chem. Chem. Phys.* **2**, 2113–2116 (2000).
- <sup>96</sup> B. R. A. Nijboer and F. W. De Wette, “The internal field in dipole lattices,” *Physica* **24**, 422–431 (1958).
- <sup>97</sup> E. Madelung, “Das elektrische feld in systemen von regelmäßig angeordneten punktladungen,” *Phys. Z.* **19**, 524–533 (1918).



- <sup>98</sup> P. P. Ewald, "Die berechnung optischer und elektrostatischer gitterpotentiale," *Ann. Phys.* **369**, 253–287 (1921).
- <sup>99</sup> S.N Stuart, "Depolarization correction for Coulomb lattice sums," *J. Comput. Phys.* **29**, 127–132 (1978).
- <sup>100</sup> Frank E. Harris, "Hartree-fock studies of electronic structures of crystalline solids," in *Theoretical Chemistry: Advances and Perspectives*, Theoretical Chemistry, Vol. 1, edited by Henry Eyring and Douglas Henderson (Academic Press, New York, 1975) pp. 147–218.
- <sup>101</sup> V. R. Saunders, C. Freyria-Fava, R. Dovesi, L. Salasco, and C. Roetti, "On the electrostatic potential in crystalline systems where the charge density is expanded in Gaussian functions," *Mol. Phys.* **77**, 629–665 (1992).
- <sup>102</sup> F. W. De Wette and B. R. A. Nijboer, "The electrostatic potential in multipole lattices," *Physica* **24**, 1105–1118 (1958).
- <sup>103</sup> Konstantin N Kudin and Gustavo E Scuseria, "A fast multipole algorithm for the efficient treatment of the Coulomb problem in electronic structure calculations of periodic systems with Gaussian orbitals," *Chem. Phys. Lett.* **289**, 611–616 (1998).
- <sup>104</sup> Konstantin N. Kudin and Gustavo E. Scuseria, "Revisiting infinite lattice sums with the periodic fast multipole method," *J. Chem. Phys.* **121**, 2886–2890 (2004).
- <sup>105</sup> A. Redlack and J. Grindlay, "Coulombic potential lattice sums," *J. Phys. Chem. Solids* **36**, 73–82 (1975).
- <sup>106</sup> James E. Roberts and Jurgen Schnitker, "How the unit cell surface charge distribution affects the energetics of ion–solvent interactions in simulations," *J. Chem. Phys.* **101**, 5024–5031 (1994).
- <sup>107</sup> Henry David Hecce, Angel Enrique Garcia, and Thomas Darden, "The electrostatic surface term: (I) periodic systems," *J. Chem. Phys.* **126**, 124106 (2007).
- <sup>108</sup> V. Ballenegger, "Communication: On the origin of the surface term in the Ewald formula," *J. Chem. Phys.* **140**, 161102 (2014).
- <sup>109</sup> Roman Lazarski, Asbjörn Manfred Burow, Lukáš Grajciar, and Marek Sierka, "Density functional theory for molecular and periodic systems using density fitting and continuous fast multipole method: Analytical gradients," *J. Comput. Chem.* **37**, 2518–2526 (2016).
- <sup>110</sup> Asbjörn M. Burow and Marek Sierka, "Linear scaling hierarchical integration scheme for the exchange-correlation term in molecular and periodic systems," *J. Chem. Theory Comput.* **7**, 3097–3104 (2011).
- <sup>111</sup> Carolin Müller, Manas Sharma, and Marek Sierka, "Real-time time-dependent density functional theory using density fitting and the continuous fast multipole method," *J. Comput. Chem.* **41**, 2573–2582 (2020).
- <sup>112</sup> Michael F. Peintinger, Daniel Vilela Oliveira, and Thomas Bredow, "Consistent gaussian basis sets of triple-zeta valence with polarization quality for solid-state calculations," *J. Comput. Chem.* **34**, 451–459 (2013).
- <sup>113</sup> Joachim Laun and Thomas Bredow, "BSSE-corrected consistent gaussian basis sets of triple-zeta valence with polarization quality of the fifth period for solid-state calculations," *J. Comput. Chem.* **43**, 839–846 (2022).
- <sup>114</sup> Florian Weigend, "Accurate coulomb-fitting basis sets for H to Rn," *Phys. Chem. Chem. Phys.* **8**, 1057–1065 (2006).
- <sup>115</sup> Kesha Sorathia and David P. Tew, "Basis set extrapolation in pair natural orbital theories," *J. Chem. Phys.* **153**, 174112 (2020).
- <sup>116</sup> Kesha Sorathia, Damyan Frantsov, and David P. Tew, "Improved CPS and CBS extrapolation of PNO-CCSD(T) energies: The MOBH35 and ISOL24 data sets," *J. Chem. Theory and Comput.* **20**, 2740–2750 (2024).
- <sup>117</sup> Florian Weigend and Marco Häser, "RI-MP2: first derivatives and global consistency," *Theor. Chem. Acc.* **97**, 331–340 (1997).
- <sup>118</sup> Sree Ganesh Balasubramani, Guo P. Chen, Sonia Coriani, Michael Diedenhofen, Marius S. Frank, Yannick J. Franzke, Filipp Furche, Robin Grotjahn, Michael E. Harding, Christof Hättig, Arnim Hellweg, Benjamin Helmich-Paris, Christof Holzer, Uwe Huniar, Martin Kaupp, Alireza Marefat Khah, Sarah Karbalaee Khani, Thomas Müller, Fabian Mack, Brian D. Nguyen, Shane M. Parker, Eva Perlt, Dmitriy Rappoport, Kevin Reiter, Saswata Roy, Matthias Rückert, Gunnar Schmitz, Marek Sierka, Enrico Tapavicza, David P. Tew, Christoph van Wüllen, Vamsee K. Voora, Florian Weigend, Artur Wodyński, and Jason M. Yu, "TURBOMOLE: Modular program suite for ab initio quantum-chemical and condensed-matter simulations," *J. Chem. Phys.* **152**, 184107 (2020).
- <sup>119</sup> Yannick J. Franzke, Christof Holzer, Josefine H. Andersen, Tomislav Begušić, Florian Bruder, Sonia Coriani, Fabio Della Sala, Eduardo Fabiano, Daniil A. Fedotov, Susanne Fürst, Sebastian Gillhuber, Robin Grotjahn, Martin Kaupp, Max Kehry, Marjan Krstić, Fabian Mack, Sourav Majumdar, Brian D. Nguyen, Shane M. Parker, Fabian Pauly, Ansgar Pausch, Eva Perlt, Gabriel S. Phun, Ahmadreza Rajabi, Dmitriy Rappoport, Bibek Samal, Tim Schrader, Manas Sharma, Enrico Tapavicza, Robert S. Treß, Vamsee Voora, Artur Wodyński, Jason M. Yu, Benedikt Zerulla, Filipp Furche, Christof Hättig, Marek Sierka, David P. Tew, and Florian Weigend, "Turbomole: Today and tomorrow," *J. Chem. Theory Comput.* **19**, 6859–6890 (2023).
- <sup>120</sup> Xiang-Lin Meng, Ning Lun, Yong-Qiu Qi, Jian-Qiang Bi, Yong-Xin Qi, Hui-Ling Zhu, Fu-Dong Han, Yu-Jun Bai, Long-Wei Yin, and Run-Hua Fan, "Low-temperature synthesis of meshy boron nitride with a large surface area," *Eur. J. Inorg. Chem.* **2010**, 3174–3178 (2010).
- <sup>121</sup> Guillaume Cassabois, Pierre Valvin, and Bernard Gil, "Hexagonal boron nitride is an indirect bandgap semiconductor," *Nat. Photonics* **10**, 262–266 (2016).
- <sup>122</sup> Anubhav Jain, Shyue Ping Ong, Geoffroy Hautier, Wei Chen, William Davidson Richards, Stephen Dacek, Shreyas Cholia, Dan Gunter, David Skinner, Gerbrand Ceder, and Kristin A. Persson, "The materials project: A materials genome approach to accelerating materials innovation," *APL Mater.* **1**, 011002 (2013).
- <sup>123</sup> F. E. Pretzel, G. N. Rupert, C. L. Mader, E. K. Storms, G. V. Gritton, and C. C. Rushing, "Properties of lithium hydride I. single crystals," *Journal of Physics and Chemistry of Solids* **16**, 10–20 (1960).
- <sup>124</sup> Xiao Li and Hongwei Zhu, "Two-dimensional MoS<sub>2</sub>: Properties, preparation, and applications," *J. Mater.* **1**, 33–44 (2015).
- <sup>125</sup> Rudren Ganatra and Qing Zhang, "Few-layer MoS<sub>2</sub>: A promising layered semiconductor," *ACS Nano* **8**, 4074–4099 (2014).
- <sup>126</sup> H. Şahin, S. Cahangirov, M. Topsakal, E. Bekaroglu, E. Akturk, R. T. Senger, and S. Ciraci, "Monolayer honeycomb structures of group-IV elements and III-V binary compounds: First-principles calculations," *Phys. Rev. B* **80**, 155453 (2009).

- <sup>127</sup> Denis Usvyat, Bartolomeo Civalleri, Lorenzo Maschio, Roberto Dovesi, Cesare Pisani, and Martin Schütz, “Approaching the theoretical limit in periodic local MP2 calculations with atomic-orbital basis sets: The case of lih,” [J. Chem. Phys.](#) **134**, 214105 (2011).
- <sup>128</sup> Lorenzo Maschio, Denis Usvyat, and Bartolomeo Civalleri, “*Ab initio* study of van der waals and hydrogen-bonded molecular crystals with a periodic local-mp2 method,” [CrystEngComm](#) **12**, 2429–2435 (2010).